ACS APPLIED MATERIALS & INTERFACES

www.acsami.org

Research Article

Radiodynamic Properties of Liposomes Encapsulating a Bi^{3+} Triple-Decker Phthalocyanine

Sofia Leo,* Elena Murillo Vilella, Laura Contini, Fabrizia Grepioni, Romain Haudecoeur, Pierre-Henri Lanoë, Malika Kadri, Marc-André Hograindleur, Eaazhisai Kandiah, Jean-Luc Coll, Lucie Sancey, Benoit Habermeyer,* and Mans Broekgaarden*

Cite This: *ACS Appl. Mater. Interfaces* 2026, 18, 16205−16221

Read Online

ACCESS | Metrics & More | Article Recommendations | Supporting Information

ABSTRACT: The development of next-generation radiosensitizing agents is of major interest for enhancing tumor-specific radiation responses while minimizing the toxicity to healthy tissues. Among emerging radiosensitizers, porphyrinoids have attracted attention, as their unique redox properties, further enhanced by specific coordination metals, can augment radiation-induced oxidative tissue damage. While porphyrins and texaphyrins have been widely investigated, it remains unclear whether phthalocyanines are similarly effective. In this work, we report on the design, synthesis, and characterization of a triple-decker bismuth−phthalocyanine complex (**BiTD**), consisting of three tetra(*t*-butyl)phthalocyanine ligands coordinated by two Bi centers. To improve biocompatibility and enhance cellular uptake, **BiTD** was encapsulated in liposomes, where it exhibited excellent stability. Under these conditions, **BiTD** significantly outperformed free phthalocyanines in radiochemical assays, generating markedly higher levels of reactive oxygen species (ROS) upon ionizing radiation. Importantly, **BiTD** also increased radiotherapy outcomes in pancreatic cancer spheroids. These results highlight bicoordinated multideck phthalocyanines as a promising metalloorganic radiosensitizer and establish a new molecular design strategy to enhance radiodynamic therapy (RDT) while facilitating the understanding of its hypothetical mechanisms and applications.

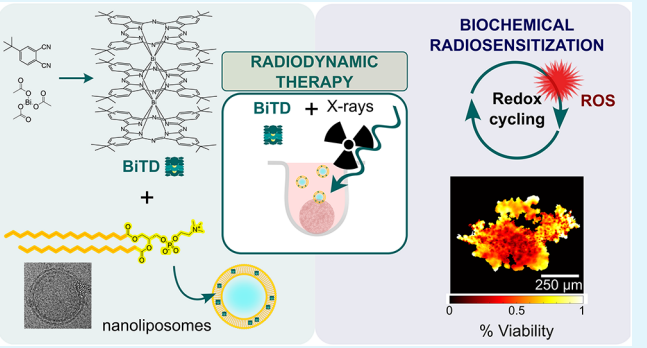

KEYWORDS: *RDT, sandwich phthalocyanines, bismuth, liposomes, radiotherapy*

Downloaded via INIST-CNRS on March 27, 2026 at 14:28:39 (UTC).
See https://pubs.acs.org/sharingguidelines for options on how to legitimately share published articles.

INTRODUCTION

Pancreatic cancer is the third leading cause of cancer-related mortality worldwide, with persistently low survival rates due to limited advancements in early diagnosis, treatment, and disease management.[1] Among treatment strategies, radiotherapy is recognized as an effective approach for controlling local tumor progression and is recommended as neoadjuvant, adjuvant or palliative treatment depending on the country and stage of the disease.[2] Although the value of radiotherapy in the treatment of pancreatic cancer has been debated,[3] it is clear that chemoradiation therapy improved survival or treatment outcomes in patients with resectable and borderline resectable disease.[4−6] More efficient radiotherapy regimes, potentially combined with radiosensitizing agents, may aid in further reducing tumor burdens and increasing successful surgical resection rates.[7]

To enhance radiotherapy efficacies while minimizing adverse events, various strategies, such as the development of particles and molecules with radiosensitizing capabilities, are being explored. High-Z nanoparticles, in particular, offer significant potential to boost radiotherapy effectiveness while minimizing harm to healthy tissues. Several high-Z metals have been studied and engineered into nanoparticles such as Au, Ag, Ti, Bi, and various lanthanides and studied for their radiocatalytic properties.[7] For example, La and Lu-based nanoparticles were recently shown to induce radiation dose-enhancement in various *in vivo* and *in vitro* models of pancreatic cancer.[8,9] While many high-Z elements belong to noble metals or rare earth categories, Bi stands out as a nonprecious element with the highest atomic number ($Z = 83$) among all nonradioactive elements, offering a unique and cost-effective alternative.[7] Bi nanoparticles have been studied as radiosensitizers, demonstrating the ability to enhance the generation of reactive oxygen species (ROS) and inhibit tumor growth *in vivo*.[7,10] Although promising, inorganic nanoparticles often face challenges due to their poor biodegradability and small size

Received: December 31, 2025
Revised: March 7, 2026
Accepted: March 8, 2026
Published: March 16, 2026

© 2026 The Authors. Published by American Chemical Society

that leads to rapid clearance from tumor sites and prolonged retention in the body, the requirement of specific coatings for biocompatibility that can influence their radiotherapeutic properties, and the necessity of high tumor concentrations to achieve radiation dose-enhancement.[7−9]

As an alternative approach to sensitize tissues to radiotherapy, porphyrinoids have gained attention as they can act as molecular radiosensitizers.[11,12] Many porphyrin-like agents can engage with hydrated electrons that are generated during radiotherapy, yielding radical anions that can trigger the formation of different types of ROS. The reduction of O_2 to form $O_2^{\bullet-}$ is a prominent example. In addition, especially metal-coordinated porphyrinoids can act as oxidizing agents in native- or radiotherapy-treated environments, thereby causing or exacerbating oxidative stress in cells and tissues. These effects elevate the overall ROS generation during radiotherapy, thereby augmenting its efficacy. Within the family of porphyrinoids, substantial research has been performed on porphyrins and texaphyrins, yet phthalocyanines have scarcely been investigated as RDT agents. Nonetheless, phthalocyanines are particularly attractive because their larger pyrrolic cavity allows efficient coordination of a wide range of metals, including high-Z elements.[13] Given the radiotherapeutic potential of Bi, we hypothesized that incorporating Bi into phthalocyanines could create an innovative radiosensitizing compound.

In this study, we describe the synthesis and radiotherapeutic potential of a novel Bicoordinated phthalocyanine. While exploring the synthesis of this compound, a unique triple-decker system composed of three tetra(*t*-butyl)phthalocyanine (**tbPc**) units coordinated by two Bi atoms, referred to as **BiTD**, has been obtained. Sandwich-type phthalocyanines, including triple-decker variants, have been well-documented for applications in optical materials, gas sensors, and molecular conductors owing to their tunable electronic properties.[14,15] However, to date, no biomedical applications such as photodynamic therapy or radiosensitization have been explored for these systems. In order to define its therapeutic potential and improve the biocompatibility of this hydrophobic compound, we explored its formulation into liposomes. **BiTD** demonstrated remarkable stability within liposomes and elevated ROS production during radiotherapy in solution. In contrast, free tetra(*t*-butyl)phthalocyanine (**tbPc**) showed no such effects, suggesting that the metal had some influence on the radiocatalytic properties of the phthalocyanines. *In vitro* assays on 3D culture models of pancreatic cancer revealed resistance to treatment, yet **BiTD** demonstrated therapeutic benefits in reducing viability and cell growth, positioning this particular complex as a promising prototype for next-generation high-Z radiosensitizers.

EXPERIMENTAL SECTION

Chemicals and Reagents

All reagents and solvents for the synthesis were obtained from Merk (Darmstadt, Germany) and VWR (Radnor, Pennsylvania). Cell culture media DMEM with GlutaMAX supplement and sterile phosphate-buffered saline (PBS) supplemented with $CaCl_2$ and $MgCl_2$ were purchased from Gibco (Thermo Scientific, Waltham, MA, USA). Fetal bovine serum was from Dominique Dutcher (FBS, Bernolshem, France). Aminophenyl fluorescein (APF), dihydroethidium (DHE), 5(6)-carboxyfluorescein (CF), 2-[4-(2-hydroxyethyl)-piperazin-1-yl]ethanesulfonic acid (HEPES, minimum 99.5% titration), sodium hydroxide (NaOH), Bismuth(III) Acetate, 1,5-diazabicyclo[5.4.0]undec-7-ene, and Triton-X have been purchased from Merck (Darmstadt, Germany). The lipids 1,2-distearoyl-*sn*-glycero-3-phosphocholine (DSPC), 1,2-dioleoyl-*sn*-glycero-3-phosphoethanolamine (DOPE), *N*-(carbonyl-methoxypolyethylene glycol-2000)-1,2-distearoyl-*sn*-glycero-3-phosphoethanolamine (DSPE-PEG), and phosphatidylcholine (content ≥ 94.0%) from Soybean (Soy-PC) were purchased from Lipoid (Ludwigshafen, Germany). Cholesterol was purchased from Sigma-Aldrich (Saint-Quentin-Fallavier, France). 1-Palmitoyl-2-{12-[(7-nitro-2−1,3-benzoxadiazol-4-yl)amino]dodecanoyl}-*sn*-glycero-3-phosphocholine (NBD-PC) was obtained from Avanti Polar Lipids (Sigma Adrich).

Synthesis of Tetra-(*t*-butyl) Phthalocyanine (tbPc)

The synthesis of tertra-(*t*-butyl) phthalocyanine (**tbPc**) is detailed in the Supporting Information.

Synthesis of BiTD

BiTD has been synthesized using the standardized *Tomoda method* for phthalocyanine synthesis.[16,17] In a two-necked flask under an argon atmosphere, 4-(*t*-butyl)phthalonitrile (1 g, 0.0054 mol) together with Bi(III)Acetate (1.5 g, 0.0038 mol) were dissolved in 2-dimethylaminoethanol (DMAE, 12.5 mL, to achieve full solubilization). Subsequently, 1,5-diazabicyclo[5.4.0]undec-7-ene (DBU, 0.809 mL, 0.0054 mol) was added to the stirring solution. The reaction mixture was refluxed and stirred for 20 h shielded from the light. Upon completion, the solution turned deep dark green/blue, with UV−vis analysis showing a spectrum composed of a strong Soret band at 348 nm and an abroad Q-band at 680 nm. Distilled water was added directly to the reaction mixture, which caused the precipitation of a dark blue/green solid. The precipitate was filtered, washed thoroughly with water to remove residual solvent and DBU, and dried. Initial attempts to purify the compound revealed its instability on SiO_2 and Al_2O_3, as these materials promoted demetalation. This instability was further influenced by the polarity of the solvent; for instance, the compound exhibited degradation over time in polar solvents like ethanol. After various purification strategies and solvent systems were evaluated, the compound was successfully isolated using size-exclusion chromatography (Bio-Beads S-X1, Hercules, California, USA) with toluene as the eluent. During the overall process, the column has been protected from light exposure. Two bands were clearly distinguished, one sky blue and another petrol green. The latter, which was the fastest eluting band corresponding to the highest molecular weight species, was collected and dried yielding 77.8 mg of a petrol green powder (6.7% yield, due to the losses encountered during the first assay of purification procedures). The product has been further characterized by ^{1}H NMR (Bruker Ultrashield 500TM, Billerica, US), UV−vis spectrophotometry (UV-1800 Shimadzu, Kyoto, Japan), and MALDI-TOF mass spectrometry (Bruker microflex). In the ^{1}HNMR characterization, a small drop of toluene was added to the NMR tube to prevent further aggregation of the triple-decker complexes. This precaution was necessary to improve the spectral resolution and more reliable assignment of proton resonances, as supramolecular aggregation can lead to broad or poorly resolved signals.

Crystals Imaging

In a glass vial 10 mg of **BiTD** were dissolved in toluene, the solution was left open and placed inside a larger Teflon vial, which was then sealed and enclosed within a stainless-steel pressure reactor. This setup was heated in an oven at 130 °C for 24 h. The system was subsequently cooled at a rate of −10 °C per hour until it reached 30 °C. After cooling, the pressure was removed, and the reactor opened, yielding an octane-green solution (matching the color of the initial powder). Over the course of 2 weeks, crystals formed spontaneously within the solution. **BiTD** crystal images were collected under polarized light using an optical microscope (Axio Imager M2, Zeiss, Oberkochen Germany) and a 20× objective (Plan-Apochromat 20*x*/0.75).

Cyclic Voltammetry Analysis

Cyclic voltammetry (CV) experiments were carried out using a Biologic SP300 potentiostat (BioLogic SAS, Seyssinet-Pariset,

https://doi.org/10.1021/acsami.5c26335
ACS Appl. Mater. Interfaces 2026, 18, 16205−16221

France) under an argon atmosphere. Measurements were performed in dry dichloromethane (CH_2Cl_2) containing 0.2 M tetrabutylammonium hexafluorophosphate ($TBAPF_6$) as the supporting electrolyte. The analyte was prepared as a 1.0 mM solution in the same medium. A conventional three-electrode configuration was used, consisting of a glassy carbon disk (3 mm diameter) as the working electrode, a platinum wire as the counter electrode, and a silver/silver nitrate (Ag/$AgNO_3$, 0.01 M in CH_3CN) electrode as the nonaqueous reference. All measurements were conducted at a scan rate of 100 mV·s^{-1}.

Liposome Preparation and Characterization

Liposomes were prepared using the lipid film-hydration method. All lipid components and sensitizer (either **BiTD** or **tbPc**) were combined at the ratios specified in Table S1. The mixtures were dried overnight by centrifugation at 1465 rpm and 40 °C, under vacuum (Genevac miVac centrifugal concentrator, Ipswich, UK). The dried films were then rehydrated with 0.5 mL of PBS to achieve a final lipid concentration of 10 mM. The rehydrated mixtures were first sonicated in a bath sonicator at 37 kHz and 60 °C (Elmasonic p30, Elma Schmidbauer GmbH, Singen, Germany) for at least 15 min until complete dissolution was achieved, followed by additional sonication using a tip sonicator in pulse mode 10 s on at 50% power, 10 s off, for a total on-time of 90 s (Fisherbrand Model 120 Sonic Dismembrator, Fischer scientific). For cell experiments, liposomes were sterilized immediately before use, keeping the samples for 15 min at 95 °C.

Liposomes Stability and Characterization

Liposomes were prepared as described above and characterized for their size, polydispersity, emission, and absorbance. The hydrodynamic diameter and polydispersity index of the liposomes were measured using dynamic light scattering (DLS) on a Zetasizer Ultra Red instrument (Malvern Panalytical, Malvern, WS, USA). Absorbance measurements were conducted with an EVOLUTION 201 UV−visible spectrophotometer (Thermo Scientific) on liposome solutions at 500 μM in PBS, and on free compounds (**BiTD** and **tbPc**) in chloroform. Fluorescence intensity was measured in Falcon 96-well transparent flat-bottom plates (Corning Inc., Corning, NY, USA), each well containing 100 μL of liposome solution in PBS at 1 mM. The fluorescence was detected using a CLARIOstar Plus plate reader (BMG Labtech, Ortenberg, Germany) with excitation at 349 ± 15 nm, emission between 680 and 730 nm, and a gain setting of 3000. Afterward the liposomes have been stocked in a fridge at 4 °C under N_2 for a period of 4 weeks. At the end of this period the fluorescence, absorbance and DLS measurements have been evaluated and compared to the initial one to evaluate any changes.

Encapsulation Efficiency

To assess the encapsulation efficiency, calibration curves were first established by using the Beer−Lambert law by measuring the absorbance of free compounds in solution across various concentrations. The encapsulated sensitizers were obtained by liquid−liquid extraction during which the liposomal samples were dissolved in chloroform. The resulting solution was analyzed for absorbance, and the concentration of encapsulated compounds was determined from the calibration curves. The encapsulation efficiency was calculated by EE % = $(C_a - C_m)$ 100/C_a where C_a is the aimed concentration and C_m is the measured concentration.

Phthalocyanine Retention

To evaluate the leakage of encapsulated sensitizers under exposure to different media, fluorescence intensity measurements were performed. Liposomes at 1 mM concentration were solubilized in five different media: PBS, DMEM, 10% FBS and 90% DMEM, 25% FBS and 75% DMEM, and pure FBS. Additional wells without liposomes were included to measure the background fluorescence. The plate was maintained at 37 °C throughout the experiment, and fluorescence intensity was recorded at time zero, 20 min, 1h, 2h, 4h, and 8h and any significant change was evaluated for each time point.

Cryo-EM

For characterization by cryoelectron microscopy, liposomes composed by DSPC:Chol:DSPE-PEG in a 66:30:4 molar ratio were prepared at a 40 mM final concentration. Three μL of the sample was applied on glow-discharged 1.2/1.3-hole sized C-Flat holey copper grids with a carbon foil (300 mesh) and plunged frozen in liquid ethane using a Vitrobot Mark IV (Thermo Fisher Scientific). Grid screening and imaging were performed on a 300 kV Titan Krios G3 on the CM01 beamline[18] at ESRF, using a K3 direct electron detector (AMETEK) in counting mode with EPU, at a nominal magnification of 130,000× (0.657 Å pixel size). Raw movies were motion-corrected using MotionCor2 software before analyzing the images for liposomes.

SAXS Diffraction

Small-angle X-ray scattering (SAXS) measurements were conducted at the SWING beamline of the SOLEIL synchrotron (Saint-Aubin, France) and analyzed as described previously.[19] Empty liposomes or liposomes containing 4 mol % phthalocyanines were prepared with the same procedure up to a concentration of 18 mg mL^{-1}. To ensure size uniformity, the liposome suspension was extruded at 80 °C through inorganic membrane filters (Whatman, 200 nm pore size, 10 mm diameter, Merck) and analyzed by DLS.

Irradiation System

Irradiation experiments were conducted using the Small Animal Radiation Research Platform (SARRP, X-Strahl, Ratingen, Germany). Samples were exposed to X-ray radiation at a maximum dose of 16 Gy, delivered with a beam set to 220 kVp, 3.07 Gy/min, and 13 mA current, utilizing a 0.15 mm copper filter. The plates were irradiated at a source-to-sample distance of 35 cm in an open irradiation field without a mounted collimator.

ROS Production Detection and Redox Assays

Aminophenyl fluorescein (APF), a fluorescent probe widely used and validated for the detection of different types of radicals, including $^{\bullet}OH$, but also $ONOO^{\bullet}$, and $^{\bullet}OCl$ radicals, in both chemical and biological systems.[20,21] Notably, its oxidation is highly specific, with minimal response to other ROS like H_2O_2 or $O_2^{\bullet-}$.[20] Solutions were prepared in 96-well flat-bottom black plates (Greiner Bio-One, Frickenhausen, Germany), with a final volume of 100 μL per well and a concentration of liposome 1 mM. Fluorescence measurements were performed by using a plate reader (FLUOstar Omega, BMG LABTECH, Ortenberg, Germany). The fluorescence was measured before and after X-ray irradiation at λ_{exc} 485 ± 10 and λ_{em} 520 ± 20 nm (FLUOstar Omega, BMG LABTECH, Champigny sur Marne, France). All reported values represent the fluorescence difference before and after irradiation. The ability of the phthalocyanine complexes to participate in redox cycling was assayed in cell-free solutions containing 1 mM of ascorbate (pH 7.4), 50 μM dehydroxyethidium, and liposomal **BiTD** or **tbPc** at varying concentrations. The total volume was 100 μL in black-walled optical 96-wells plates (Corning). The reactions were incubated at 37 °C for 24 h, during which emission spectra of 2-hydroxyethidium (λ_{ex} 510 ± 16 nm, λ_{em} 538−700 ± 10 nm) were measured following 24 h incubation at 37 °C.

Carboxyfluorescein Release

To assess ROS generation within the liposomal membranes, the release of hydrophilic carboxyfluorescein (CF) was assayed. CF was loaded at a self-quenching concentration of 57 mM (HEPES buffer, pH 7.4).[22] Liposome solutions were prepared at 1 mM in PBS, with 10 μL per well in two identical 96-well flat-bottomed black plates (Corning). At time zero, the plates were incubated at 37 °C. After 30 min, one plate was irradiated with X-rays at 4 Gy, while the other plate served as a control. CF release was quantified using fluorescence spectroscopy with a FLUOstar Omega plate reader (FLUOstar Omega, BMG LABTECH, Champigny sur Marne, France). Measurements were performed with excitation at λ_{exc} 485 ± 10 nm and λ_{em} 520 ± 20 nm (gain 600). Initial CF emission was recorded at time zero, followed by periodic measurements at 30 min, 1.5, 2.5, 17.5, and 24 h to generate time-dependent release curves. To ensure the complete release of CF, liposomes were disrupted by adding Triton X-100 (Sigma-Aldrich) to a final concentration of 0.01% (v/v). The

https://doi.org/10.1021/acsami.5c26335
ACS Appl. Mater. Interfaces 2026, 18, 16205−16221

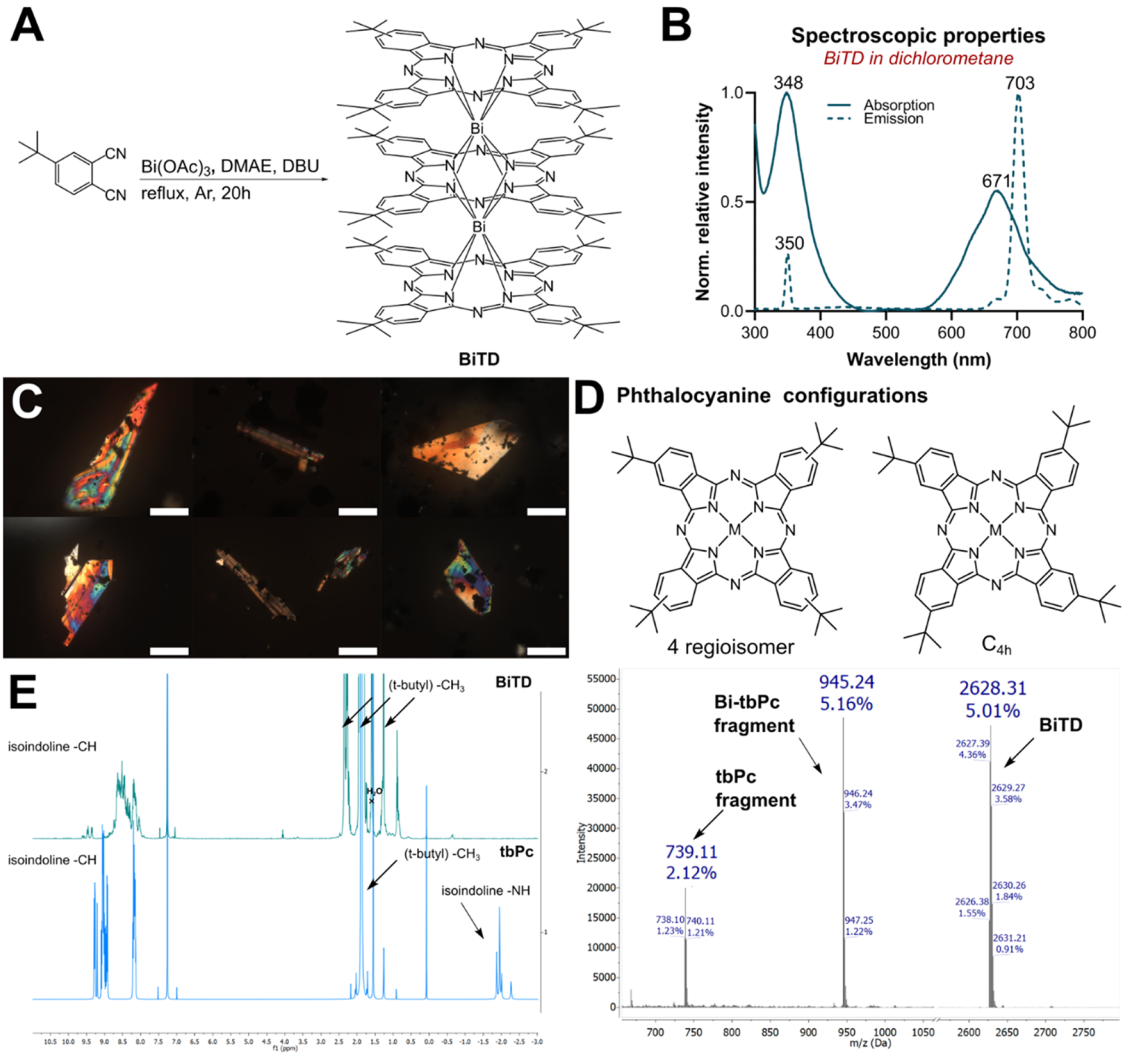

Figure 1. Physicochemical characterization of **BiTD**. (A) Schematic of the synthesis of the compound. (B) Absorption and emission spectra of **BiTD**. (C) Crystal images obtained through solvothermal synthesis and imaged under polarized light. Scale bar: 200 μm. The different colors arise from birefringence, reflecting variations in optical orientation across different crystal planes. (D) Possible configurations with tetra-t butyl groups in different positions. (E) ^{1}H NMR and MALDI-TOF of **BiTD**.

percentage of dye release upon radiation exposure was calculated using the formula: $((F - F_0) \times 100)/((F_t - F_0))$ where F represents the fluorescence intensity after exposure to irradiation, F_0 and F_t denotes the intensities before the experimental conditions and after Triton X-100 treatment, respectively.

3D Cell Culture

MIA PaCa-2 (CRL-1420) and PANC-1 (CRL-1469) pancreatic cancer cell line was obtained from the American Type Culture Collection (ATCC) and used between passages 2−25. Cells were cultured, respectively, in DMEM medium, comprising 10% FBS and 1% Penicillin Streptomycin solution containing 10,000 Units/mL Penicillin and 10,000 μg/mL Streptomycin (Thermo Scientific). Prior to use, cell cultures were maintained in a humidified incubator at 37 °C with 5% CO_2. Cells were routinely checked for mycoplasma contamination (MycoAlert Mycoplasma Detection Kit, Lonza, Basel, Switzerland) and tested negative during all reported experiments.

Assessment of Liposomal Uptake in Pancreatic Cancer Spheroids

To evaluate the uptake of liposomes by spheroids, NBD-PC was included in the liposomal formulation, and its fluorescence intensity was used as indicator. PANC-1 and MIA PaCa-2 cells were seeded at a density of 5000 and 2500 cells per well, respectively, in a volume of 50 μL. For each incubation time point (1, 2, 4, 8, 16, and 24 h), a set of five samples were prepared. Additionally, a nontreated group was added as control. Liposomes before treatment were sterilized by exposing them at 95 °C for a total of 15 min. The following day, 50 μL of sterilized liposomes at 0.5 mM in DMEM were added in each well, obtaining a final concentration of 0.25 mM. After each incubation time, samples were washed twice with PBS. Spheroids were imaged using widefield fluorescence microscopy (MICA microhub, Leica Microsystems, Wetzlar, Germany), using a 10x objective (PL FLUOTAR 10x/0.32) at $\lambda_{ex/em}$ = 470/531 nm. Images were treated using a custom developed image analysis procedure in MATLAB (Mathworks, Natick, MA).[23] First, spheroid areas were extracted using adaptive thresholding to binarize each image. Then, background fluorescence intensities were obtained from the inverse masks of the nontreated spheroids and subtracted from each image. The mean fluorescence intensity in the masked images, i.e., the region of interest, was then calculated and reported.

Evaluation of Treatment Efficacies in Pancreatic Cancer Spheroids

MIA PaCa-2 (American Type Culture Collection ATPP, CRM-CRL-1420), PANC-1 (ATCC CRL-1469), and SW1990 cells (ATCC CRL-2172), were cultured in fully supplemented DMEM. Whereas MIA PaCa-2 and PANC-1 are p53 mutated,[24] SW1990 cells carry wild-type p53.[25] Cells were seeded at a density of 2500 cells per well

https://doi.org/10.1021/acsami.5c26335
ACS Appl. Mater. Interfaces 2026, 18, 16205−16221

in a volume of 50 μL. The following day, treatment began by adding 50 μL of purified liposomes at 2 mM in DMEM to each well, resulting in a final concentration of 1 mM. A nontreated group was included as a control. After 16 h, one plate was irradiated with X-rays at 8 Gy, while a second identical plate remained unirradiated as a negative control. Spheroid growth was determined by daily brightfield imaging (MICA microhub, Leica). Image acquisition was performed using a 10× objective (PL FLUOTAR 10x/0.32). Spheroid areas were extracted from the brightfield images using a custom-written script in MATLAB 2024a.[23] After 7 days post-treatment, the spheroids were exposed to a solution containing 2 μM calcein AM (Invitrogen) and a 3 μM solution of propidium iodide (Sigma-Aldrich) for 30 min. Cellular viability was evaluated using confocal laser scanning microscopy (MICA microhub, Leica), using a 10× objective (PL FLUOTAR 10x/0.32) at $\lambda_{ex/em}$= 515/495 nm and $\lambda_{ex/em}$ = 538/617 nm, respectively. Subsequent image analyses were carried out using MATLAB 2024a as described previously.[23]

SW1990 spheroid cultures were established and treated as described for MIA PaCa-2 and PANC-1 spheroids. On day 8, instead of undergoing live/dead staining, the spheroids were lysed for ATP quantification using the Celltiter Glo 3D assay (Promega, Charbonnières-les-Bains, France). The assay was performed according to the manufacturer's instructions, and luminescence was read on a Clariostar Omega (BMG labtech). Data for all treatment groups at 8 Gy were expressed as a fraction of their 0 Gy controls.

Statistical Analysis

All data were statistically analyzed in Graphpad Prism 8 (San Diego, CA, USA). The hydrodynamic diameter and polydispersity index (PDI) and viability and necrosis of spheroids were analyzed using a one-way ANOVA followed by Tukey's test for multiple comparisons. ROS production data sets were analyzed using a two-way ANOVA followed by Dunett's test for multiple comparisons. Drug release and surviving fraction of colonies were analyzed using a one-way ANOVA followed by Dunnet's test for multiple comparisons. Statistical significance is indicated as nonsignificant (ns) for $p > 0.05$, for *$p \leq 0.05$, for **$p \leq 0.01$, for ***$p \leq 0.001$, and for ****$p \leq 0.0001$. Encapsulation efficiency was fitted by using a linear regression constrained to pass through the origin. Nonlinear regressions were used to fit spheroid growth curves (logistic growth) and uptake analysis (one-phase association).

RESULTS AND DISCUSSION

Characterization and Structural Elucidation of a Triple-Decker Bismuth Phthalocyanine

The compound **BiTD** was synthesized via the tetracyclomerization of 4-*tert*-butylphthalonitrile together with Bi(III)-acetate in DMAE, selected as a high-boiling solvent (Figure 1A). However, due to the large ionic radius of Bi^{3+} (>1.03 Å) and its coordination preferences, the reaction likely favored the formation of higher-order assemblies.[26] This behavior is consistent with that reported for large-radius lanthanide ions (e.g., La^{3+}–Nd^{3+}, ionic radii >1.0 Å), which preferentially form double- and triple-decker phthalocyanine sandwich complexes. As a result, under the conditions employed, the reaction preferentially led to the formation of a sandwiched triple-decker structure rather than a single-decker bismuth phthalocyanine.[27] Spectroscopic analysis further indicated the formation of an unexpected compound distinct from a phthalocyanine monomer, as suggested by its unique absorption spectrum. The spectrum showed a high-energy Soret band at 348 nm and a low-energy Q-band at 671 nm (Figures 1B, and S6), deviating significantly from typical monomeric profiles (Figure S2).[28] The compound exhibited pronounced instability upon light exposure and during conventional purification procedures, such as silica or alumina gel chromatography. After systematic evaluation of alternative conditions, efficient purification without detectable degradation was achieved using size-exclusion chromatography, performed under protection from direct daylight and with toluene as the eluent. To further investigate the structure of this novel compound, solvothermal crystallization was attempted in order to obtain crystals suitable for X-ray diffraction analysis. The resulting crystals, with average dimensions of approximately 242 μm, exhibited irregular platelet- and needle-like morphologies and remained relatively small (Figure 1C) rendering the analysis challenging (see SI, Figure S7). Notably, the presence of multiple regioisomers is expected to hinder the growth of well-defined single crystals, as dynamic disorder arising from the undefined positioning of the *tert*-butyl substituents prevents the formation of a unique, periodic crystal lattice (Figure 1D).[29] The nature of a triple-decker arrangement significantly increased the complexity as the total number of possible configurations increased to 64, further amplifying the disorder.

^{1}H NMR analysis provided additional insights, showing a spectrum markedly different from monomeric phthalocyanines like **tbPc**. The disappearance of the isonindoline N–H signal and the emergence of three intense peaks between 0.5 and 2.5 ppm were observed, highlighting the presence of a metalated system with three possible different layers (Figure 1E). However, the exact positioning of the *tert*-butyl groups remains unresolved, and multiplet peaks and signal broadening (Figures S3 and S4) observed for the *tert*-butyl groups further support the molecule's structural disorder. MALDI-TOF analysis revealed a peak consistent with a triple-decker system (Figures 1E and S5), confirming that the highest molecular weight compound isolated via size exclusion chromatography consists of three tetra(*t*-butyl)phthalocyanine units interspersed with two bismuth atoms. Taken together, these data confirm the formation of a novel triple-decker phthalocyanine complexed with two Bi^{3+} atoms.

Redox Potentials of BiTD and tbPc

In order to evaluate the potential of these compounds to undergo redox reactions within a cellular environment, the redox properties of **BiTD** in comparison with the free-base (**tbPc**) were investigated via cyclic voltammetry. All compounds exhibit two principal, reversible or quasi-reversible reduction waves between −1.01 and −1.78 V vs $Ag/AgNO_3$, corresponding to sequential tetrapyrrole-centered reductions of the phthalocyanine ring (Table 1). The monomeric phthalocyanine displays two well-defined, reversible waves corresponding to sequential ligand-centered reductions. The first process is likely attributable to conversion of the neutral macrocycle into the radical anion ($Pc^0 \rightarrow Pc^{\bullet -}$), while the second reduction yields the dianion ($Pc^{\bullet -} \rightarrow Pc^{2-}$) (Figure 2A). Both processes are sharp, symmetric, and characteristic of a stable conjugated aromatic system undergoing localized electron uptake. By contrast, **BiTD** showed at least three reduction events. The appearance of a third reduction event in the triple-decker may reflect additional stabilization of reduced states across the extended π-system, and possible minor contributions from the Bi centers, which can modulate charge distribution. These waves are broader and more complex, corresponding to sequential, one-electron reductions attributable to the stacked phthalocyanine rings in a triple-decker motif. The progressive separation of the reduction peaks is indicative of strong electronic communication between the tetrapyrrole macrocycles and the bismuth centers, with the first

https://doi.org/10.1021/acsami.5c26335
ACS Appl. Mater. Interfaces 2026, 18, 16205−16221

Table 1. Comparative Electrochemical Properties of tbPc and BiTD[a]

property/feature	**tbPc** (free base)	**BiTD** (Bi^{3+})
metal center	none	Bi(III)
first reduction	−1.44 V	−1.78 V
second reduction	−1.04 V	−1.43 V
third reduction		−1.01 V
first oxidation	+0.29 V	+ 0.01 V
second oxidation	+0.74 V	+ 0.39 V
third oxidation	+1.18 V	+ 0.69 V
4th oxidation		+ 1.00 V
5th oxidation		+ 1.22 V
metal-centered redox		
peak shape and resolution	sharp, well-defined	broader, partially overlapping
reversibility	mostly reversible	quasi-reversible/partially reversible
electrochemical stability	high	moderate (broader processes)
electronic effects	localized on single ring	delocalized across stacked ligands; Bi influence

[a]Reported values correspond to redox potentials (vs. $Ag/AgNO_3$) obtained from cyclic voltammetry.

reduction event occurring at a significantly more positive potential than the subsequent two, in line with observations for multidecker phthalocyanines containing lanthanides or transition metals, where stepwise electron transfer to individual decks is readily observed.[30,31]

In the oxidative region, free-base **tbPc** and **BiTD** both exhibited multiple, well-resolved oxidation waves (Figure 2A,B). For **tbPc**, three distinct oxidation events are observed at +0.29 V, + 0.74 V, and +1.18 V (Table 1), likely corresponding to stepwise oxidations of the macrocycle: from Pc^0 to $Pc^{\bullet+}$, then to Pc^{2+}, and possibly involving deeper π-system oxidation at higher potential (Figure 2A). In contrast, **BiTD** exhibited broader and partially overlapping oxidative waves, reflecting the sequential extraction of electrons from the three phthalocyanine units and demonstrating the reversibility and independence of each oxidation event in the triple-decker system. The clear separation between oxidation processes supports the presence of discrete redox-active centers, modulated by the bismuth atoms, which influence the redox potentials and interval splitting. Although not previously reported for similar Bi complexes, this behavior is well-known for related metallophthalocyanine multiple-deckers, where the longitudinal extension of the π-system leads to an increase in the number of observable waves[30,32] (Figure 2B).

Taken together, these data establish that the redox activity of both systems is primarily phthalocyanine-centered but with important distinctions. The monomeric **tbPc** exhibits a classical phthalocyanine electrochemical signature, defined by two clean reductions and two to three oxidations. In contrast, **BiTD** displays a richer and more delocalized redox chemistry. The presence of an extended π-system and additional metal centers supports the stabilization of higher oxidation and reduction states. This may translate to greater tunability of potential for multielectron transfer processes, a key advantage over single phthalocyanine systems.

Encapsulation and Stabilization of BiTD in Liposomes

To obtain a highly stable and well-packed lipid bilayer we selected a DSPC:Chol:DSPE-PEG formulation, as DSPC provides the formation of a rigid bilayer, cholesterol enhances membrane packing and mechanical stability, and DSPE-PEG imparts steric stabilization.[33] Liposomes were formulated to encapsulate varying amounts of **tbPc** and **BiTD**, with the **tbPc** concentration set three times higher than that of **BiTD** to directly compare the effect of Bi insertion between the three **tbPc** decks (Table S1). The resulting liposomes formed

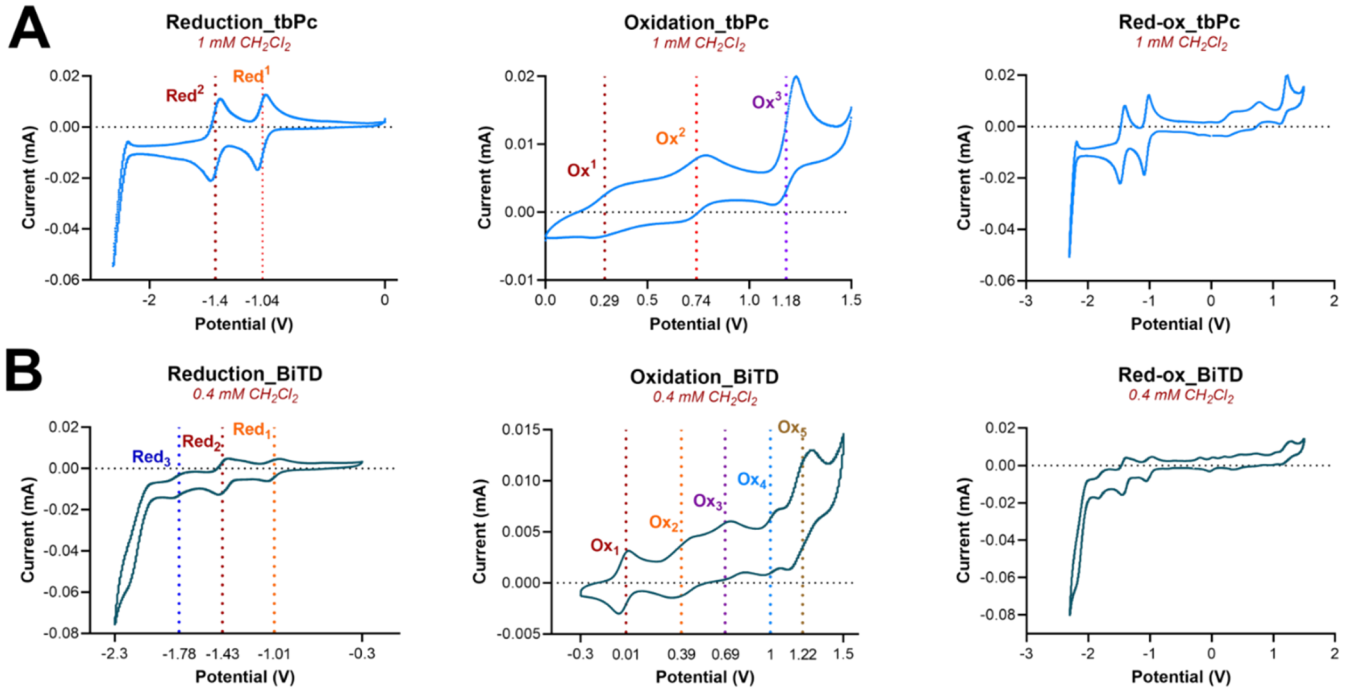

Figure 2. Cyclic voltammograms of **tbPc** and **BiTD** under argon in CH_2Cl_2 with 0.2 M TBAPF6. Panels show from left to right oxidation, reduction and full redox cycle of **tbPc** (A) and **BiTD** (B).

https://doi.org/10.1021/acsami.5c26335
ACS Appl. Mater. Interfaces 2026, 18, 16205−16221

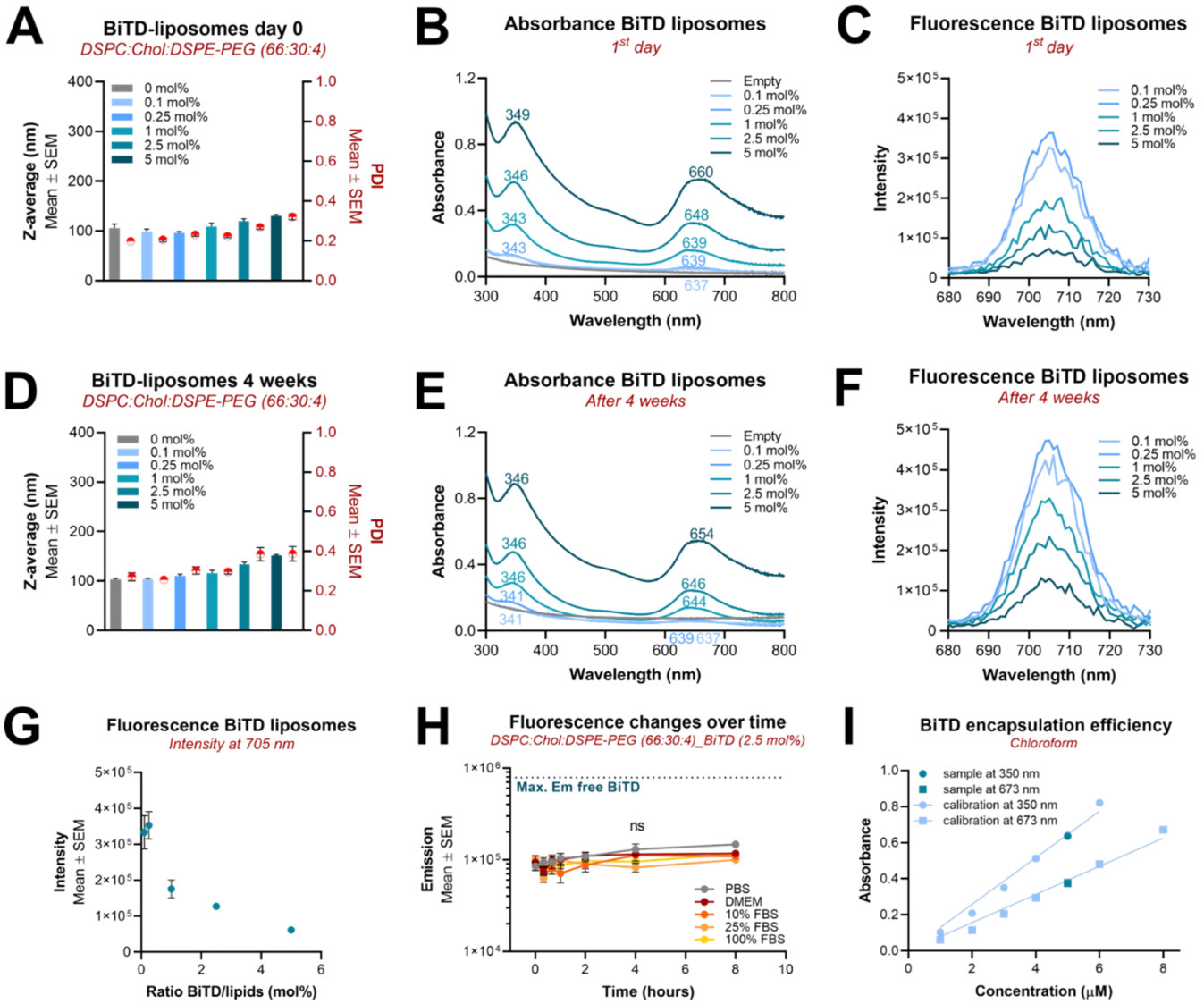

Figure 3. BiTD liposomes characterization. (A–C) Size and PDI, absorbance and emission at different mol % of **BiTD** as soon after liposomes preparation. (D–F) Size and PDI, absorbance and emission at different mol % of **BiTD** liposomes 4 weeks after liposomes preparation. Absorption results correspond to a single measurement, and all emission results are the average of triplicate measures from two technical repeats (total of N = 6). (G) Fluorescence quenching of **BiTD** when encapsulated at different concentrations into liposomes. (H) Fluorescence variation over time of **BiTD** liposomes when exposed to different media. (I) Calibration curves constructed using different absorbance peaks of **BiTD**. Data points represent the measured absorbance of destroyed liposomes containing 2.5 mol % **BiTD**, with a phthalocyanine concentration fixed at 5 μM. Assuming 100% encapsulation efficiency, the deduced sensitizer concentration for each sample would be 5 μM. Data represent the mean ± SEM of a single experiment (N = 4).

colloidally stable nanoparticles with diameters of 90–170 nm (Figure 3A), which remained stable for up to one month after synthesis (Figure 3D). UV–Vis absorbance showed only a partial decrease after 4 weeks, without significant spectral changes (Figure 3B,E). In contrast, the fluorescence intensity increased by ∼1.3-fold over the same period (Figure 3C,F). This enhancement is likely due to partial degradation of **BiTD** into monodecker **tbPc**, which displays a fluorescence intensity more than ten times higher than that of the triple-decker structure measured under the same experimental condition (Figure S9B). Fluorescence measurements also revealed quenching when the **BiTD** content exceeded 1 mol % (Figure 3G). Exploiting this property, **BiTD** leaching under different experimental conditions was evaluated. Liposomes were incubated with increasing concentrations of bovine serum, and fluorescence was monitored over time. No significant changes were observed (Figure 3H), indicating that **BiTD** was efficiently retained within the liposomal membrane, regardless of serum protein presence. Furthermore, upon liposome disruption, the absorbance values aligned precisely with the calibration curve, confirming that the recovered **BiTD** concentration matched the expected loading (Figure 3I). This demonstrates that liposome preparation preserved compound stability and prevented degradation immediately after synthesis. To further avoid any potential degradation during storage, all biochemical assays were performed with freshly prepared liposome batches, assuring a small size and PDI by DLS analysis.

Although the liposomes encapsulating the compounds were stable, certain conditions were found to promote **BiTD**

https://doi.org/10.1021/acsami.5c26335
ACS Appl. Mater. Interfaces 2026, 18, 16205–16221

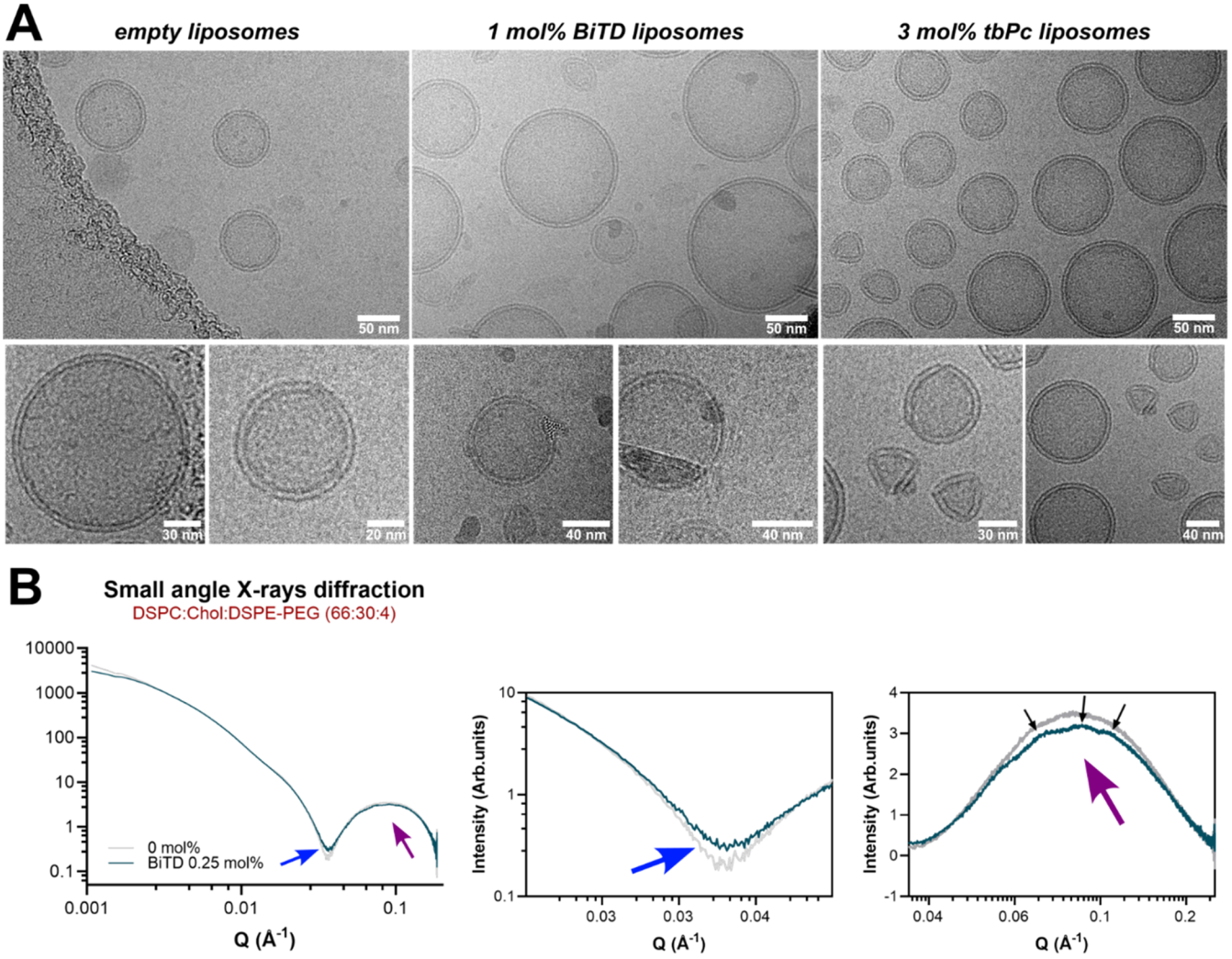

Figure 4. Structural analysis of **BiTD**-loaded liposomes. (A) Cryo-EM analysis of liposomes formulated with DSPC:Chol:DSPE-PEG in 66:30:4 molar ratio. Panels from left to right show empty, 1 mol % **BiTD** and 3 mol % **tbPc** liposomes, respectively. Images show predominantly small, spherical, and well-defined liposomes. Images in the bottom panel represent the zoom in of some liposomes, specifically highlighting particular nanostructures observed for **BiTD** and triangular-like shape liposomes observed for **tbPc**. (B) SAXS scattering curves of empty and **BiTD**-loaded liposomes, with two zoomed-in views highlighting the bilayer structural region.

degradation. For instance, when liposomes were prepared by solubilizing all components in ethanol instead of chloroform, the absorption spectra displayed partial **BiTD** degradation, as indicated by **tbPc**-like spectral features (Figure S10B–C). In contrast, chloroform-based preparations showed minimal spectral changes, likely due to its moderately polar, aprotic characteristics with a low dielectric constant (4.81 vs 24.5 for EtOH). As a result, chloroform preserves the integrity of fragile coordination complexes such as **BiTD**. NMR analyses of destroyed liposomes confirmed that **BiTD** remained intact, supporting the protective effect of the liposomal environment. These findings are consistent with previous reports on related Bi triple-decker phthalocyanines, which exhibited instability under daylight exposure but remained stable when stored below 10 °C and protected from light.[28−30] To date, no studies have systematically examined the stability of **BiTD** across different solvent types. Further details are provided in the Supporting Information (Figure S10D,E).

Cryo-EM and SAXS Analysis Confirmed the Presence of Clustered Structures in the Lipid Bilayer

The Cryo-EM micrographs in the top panel show that the DSPC:Chol:DSPE-PEG liposomes were mostly small, spherical, and well-defined (Figure 4A) consistent with the hydrodynamic diameters obtained by DLS (Figure 3A). Most vesicles display the expected unilamellar morphology and smooth membrane contours, confirming the structural stability of the formulation. In a subset of liposomes, denser or bulkier internal features can be observed, which can be attributed to the encapsulated **BiTD**, reflecting its bulkier structure within the lipid bilayer (Figure 4A).

In addition to conventional vesicles, lipodisk-like structures were also detected. Notably, the presence of a discernible lumen in some of these objects indicates that they may correspond to flattened or squeezed liposomes rather than fully formed lipodisks (Figure S8). These discoidal assemblies were observed in both empty and phthalocyanine-loaded formulations, in agreement with reports that high DSPC content can promote lipodisk formation.[34] While the bulky architecture of **BiTD** and the intrinsic aggregation tendency of phthalocya-

https://doi.org/10.1021/acsami.5c26335
ACS Appl. Mater. Interfaces 2026, 18, 16205−16221

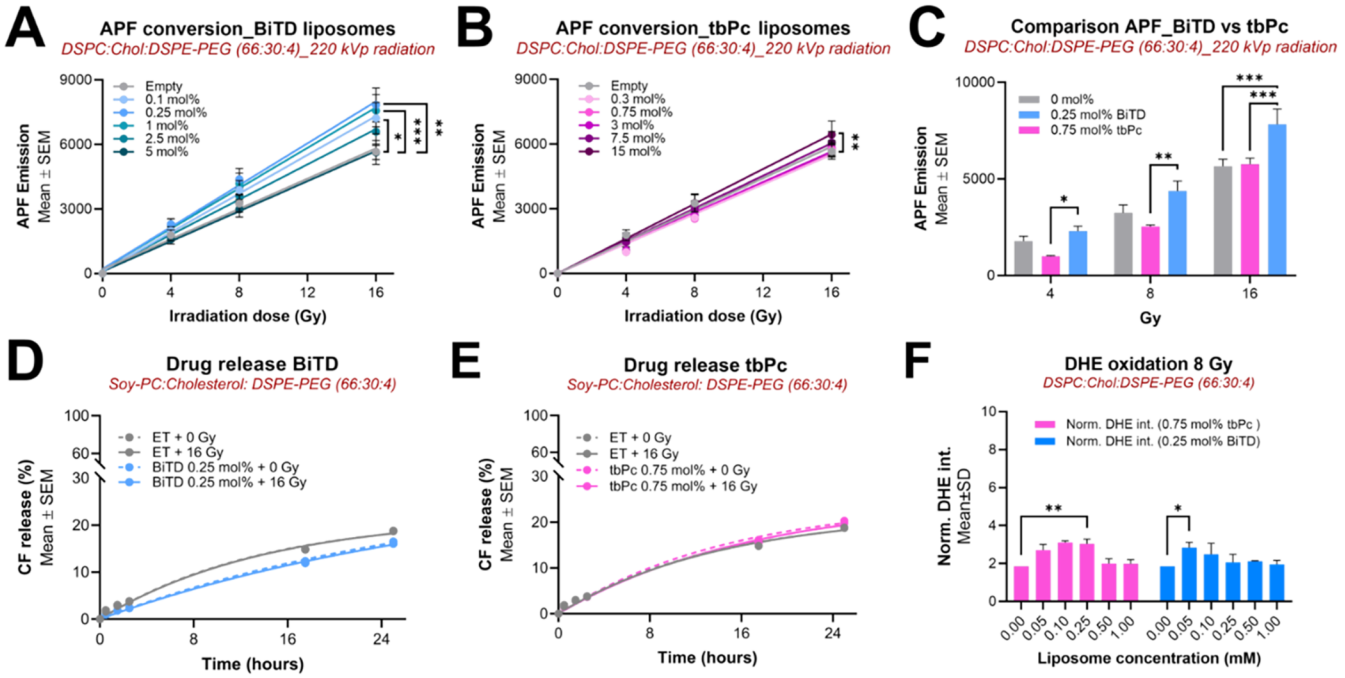

Figure 5. ROS production upon X-ray radiation (220 kVp, 3.07 Gy/min, 13 mA, 4, 8, 16 Gy). (A, B) ROS production by liposomes (DSPC:Chol:DSPE-PEG) loaded with various concentrations of **BiTD** or **tbPc** evaluated by the florescence increase of the probes (APF). (C) APF conversion comparison between liposomes loaded with **BiTD** (blue) or **tbPc** (purple). Data represent the mean ± SEM of three technical repeats (N = 9). (D, E) CF release by liposomes (Soy-PC:Chol:DSPE-PEG) with **BiTD** and **tbPc** after X-ray irradiation (220 kVp, 3.07 Gy/min, 13 mA, 16 Gy). Data represent the mean ± SEM of a single experiment (N = 6). (F) Normalized DHE oxidation after exposing the probe to **tbPc** or **BiTD** liposomes, ascorbic acid and 8 Gy radiation. Data represent the mean ± SEM of a single experiment (N = 3).

nines may further favor the emergence of these structures, their presence even in empty liposomes underscores the central role of DSPC in driving lipodisk-like vesicle formation.

SAXS analysis revealed a characteristic diffraction pattern typical of liposomal structures. In the low-q region (0.001−0.03 $Å^{-1}$), which corresponds to the overall shape and size of the liposomes,[35] no significant differences were observed between the two formulations. The liposome sizes appeared comparable, with a radius of Gyration (R_g) equal to 640 ± 29 Å, in agreement with the DLS results. In contrast, within the q-range associated with the bilayer structure and organization, the scattering profile of the **BiTD**-loaded liposomes showed a slight increase in intensity (blue arrow, Figure 4B), likely attributable to the presence of bismuth. Additionally, three small peaks were observed at $q \approx 0.1$ $Å^{-1}$ (violet arrow, Figure 4B). The origin of these features remains uncertain, but their periodic nature suggests a repeating structural motif within the lipid bilayer, which might be related to the presence of the stacked (three-deck) phthalocyanine units incorporated into the membrane. Overall, these results show that despite its bulkier architecture, **BiTD** can be effectively accommodated within the lipid bilayer without compromising liposome size or structural stability. Nonetheless, extraliposomal aggregates of **BiTD** and **tbPc** were occasionally observed when high mol % of loading was attempted, indicating that saturation of the lipid bilayers may have occurred.

BiTD, but Not tbPc, Elevated ROS Production Upon X-ray Irradiation

To further investigate the effects of **BiTD**-loaded liposomes, we evaluated their ability to catalyze ROS generation under X-ray irradiation. Liposomes containing 0.25 mol % **BiTD** significantly enhanced the X-ray−induced hydrolysis of APF to fluorescein compared to empty liposomes (Figure 5A). In contrast, **tbPc** did not exhibit detectable radiocatalytic activity, with a minimal yet statistically significant increase observed only at the much higher loading of 15 mol % (Figure 5B). Importantly, **BiTD** achieved superior performance, as even at 0.25 mol % it generated more ROS than **tbPc** at 0.75 mol % (Figure 5C). To note, the concentration of **tbPc** was 3-times higher in all of the assays to keep the number of phthalocyanines units constant between the **tbPc** and **BiTD**.

To evaluate whether the elevated ROS levels were capable of destabilizing the lipid bilayer, the formulation has been modified by substituting DSPC with SoyPC, which contains various unsaturated phosphocholines. The results demonstrated no significant increase in release compared to empty liposomes in combination with radiotherapy, demonstrating that **BiTD** or **tbPc** were not destabilizing membrane permeability (Figure 5D,E). Therefore, we hypothesized that the overall mechanisms concerning the oxidative processes observed with APF might be based on other processes likely related to the redox potential of the compound. To further assess the influence of the redox potential on the oxidative processes, **BiTD** and **tbPc** liposomes have been exposed to a solution containing DHE in the presence of ascorbic acid. Ascorbate is a well-established biological reductant ($E^{\circ\prime} \approx$ +0.28−0.33 V vs NHE at pH 7), and many metal complexes or conjugated macrocycles with more positive redox potentials can catalyze or mediate its oxidation.[36,37] The recorded redox potentials (Table 1) lie well above the ascorbate couple, supporting the hypothesis of both compounds acting as thermodynamically competent oxidants for ascorbate, rather than relying solely on oxygen as the terminal oxidant. To evaluate so, liposomes were placed in a reaction mixture with

https://doi.org/10.1021/acsami.5c26335
ACS Appl. Mater. Interfaces 2026, 18, 16205−16221

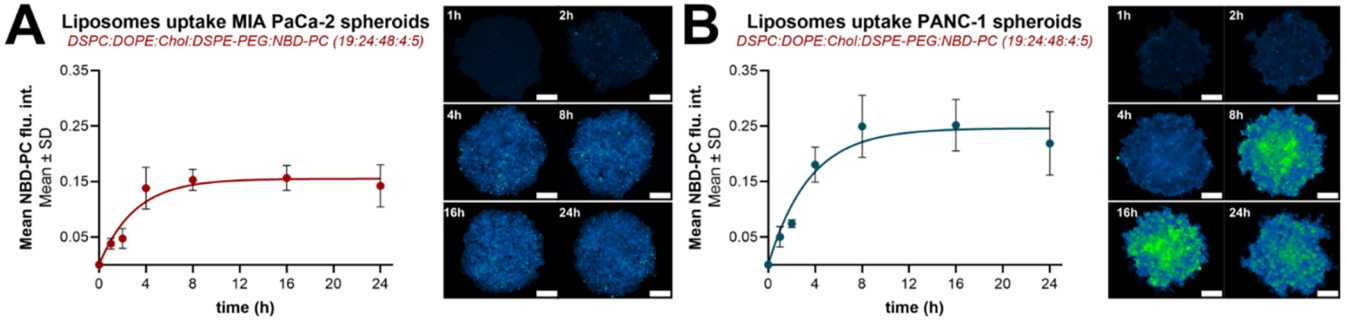

Figure 6. Time-dependent penetration of fluorescently labeled liposomes into pancreatic cancer spheroids. (A) Time-dependent uptake by MIA PaCa-2 spheroids. (B) Time-dependent uptake by PANC-1 spheroids. Representative confocal images show progressive liposome penetration into spheroids at different time points (1−24 h). Data represent the mean ± SD of two separate technical repeats with N = 8. Scale bar = 250 μm.

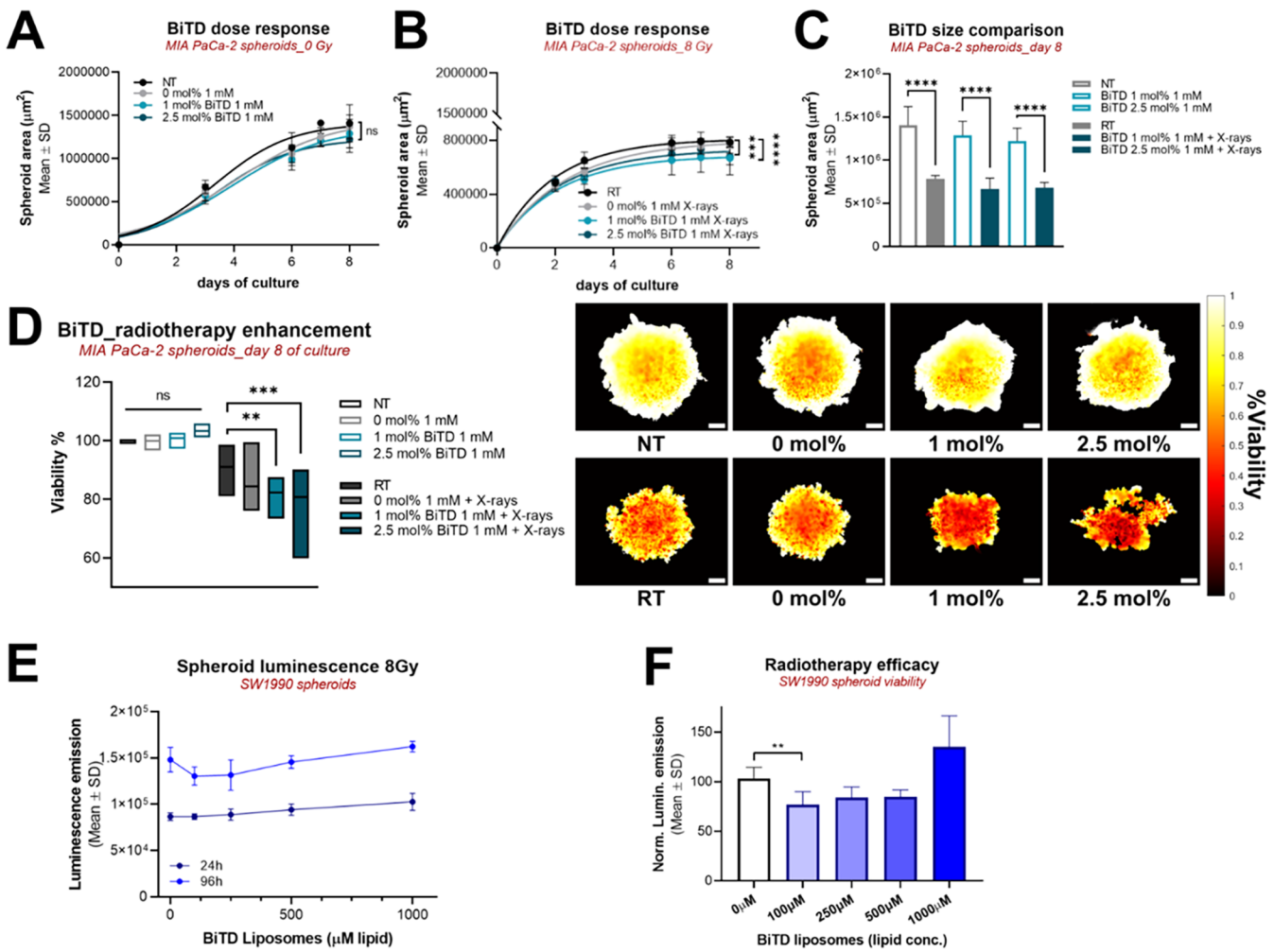

Figure 7. Effect of **BiTD**-loaded liposomes on pancreatic cancer spheroids under X-ray irradiation (220 kVp, 3.07 Gy/min, 13 mA, 8 Gy). (A−C) Growth curves and size comparison of MIA PaCa-2 compared to untreated controls. (D) Floating bars show relative viability inhibition at day 8 of culture, while representative spheroid images illustrate differences in morphology and size across conditions. Heat maps correspond to viability distributions within spheroids, with the color scale indicating live (yellow/white) to dead (red/black) cell populations. Data represent the mean ± SD of four separate technical repeat with N = 15. Scale bar = 250 μm. (E) SW1990 spheroid luminescence response after 24 (dark blue) and 96 h (blue) treated at various **BiTD** liposome concentrations. (F) Effects of radiotherapy on SW1990 spheroids at different **BiTD** liposome concentrations 96 h postradiotherapy. Data represent the mean ± SD of two separate technical repeat with N = 9−10.

ascorbic acid, and ROS generation was quantified in absence and presence of X-ray radiation using DHE, a probe sensitive to $O_2^{\bullet-}$ and H_2O_2.[38] Upon irradiation, **tbPc** and **BiTD** produced a modest yet statistically significant increase in DHE oxidation in the presence of ascorbate, further supporting the involvement of radio-induced redox cycling and ascorbate-driven ROS generation (Figure 5F). Interestingly, increasing the liposome concentrations attenuated this effect, suggesting additional competitive or self--quenching pathways at higher macrocycle concentrations, which may limit the net rate of

https://doi.org/10.1021/acsami.5c26335
ACS Appl. Mater. Interfaces 2026, 18, 16205−16221

ascorbate oxidation under these conditions. Overall, **BiTD** demonstrated clear advantages: lower concentrations not only improved radiocatalytic efficiency but also yielded smaller, more monodisperse liposomes (Figure 3A), highlighting its potential for X-ray–activated therapeutic applications.

Liposomal Uptake Kinetics in Pancreatic Cancer Spheroids

MIAPaCa-2 and PANC-1 are poorly differentiated and highly aggressive pancreatic cancer cell lines, making them well-suited for *in vitro* studies modeling tumor heterogeneity, stemness, and drug response in pancreatic ductal adenocarcinoma, thus they were chosen as model for our experiments.[39] To increase the interaction of liposomes with cells, 24 mol % of DSPC was replaced with DOPE, as is reported to confer fusogenic properties and improve overall cellular uptake.[40]

To evaluate the uptake of the formulation in 3D tumor models, the fluorescence of a lipid-anchored NBD dye was monitored over time. Liposomes showed detectable internalization after 1 h, reaching a plateau after 8 h in both cell lines (Figure 6A,B). Based on these results, subsequent experiments using **BiTD** liposomes were designed with a minimum incubation period of 8 h prior to application of the radiation treatment.

NBD-PC also demonstrated differences in fluorescence intensity between the two cell lines with the detector and laser set with equal parameters. Up to 4 h of exposure, no significant changes in fluorescence were observed in either cell line. However, after 8 h, the fluorescence intensity in PANC-1 spheroids was approximately 1.6-fold higher. While this increase could be partly attributed to differences in liposome uptake over time, it is more likely related to oxidative processes, considering the sensitivity of NBD-PC to oxidation and the distinct hypoxic characteristics of PANC-1 compared to MIA PaCa-2 spheroids.[41]

BiTD Enhanced Radiotherapy Efficacy in Pancreatic Cancer Spheroids

Given their radiocatalytic properties, retention in liposomes (Figure 3H) excellent biocompatibility, and efficient uptake of the liposomes, we next investigated whether **BiTD** could improve radiotherapy outcomes in spheroid models of pancreatic cancer. To finely control the **BiTD** dose delivered to spheroids, liposomes containing 1 or 2.5 mol % **BiTD** were administered at varying liposome concentrations. In the absence of radiation, neither empty liposomes nor **BiTD**-loaded liposomes caused notable toxicity in PANC-1 and MIA PaCa-2 spheroids, as determined by viability and spheroid growth assessment (Figures 7 and S11). In combination with radiotherapy, PANC-1 spheroids displayed a 1.9-fold reduction in overall size following RT, although there were no significant differences between RT and the combination of RT with **BiTD** liposomes (Figure S11B). In contrast, MIA PaCa-2 spheroids showed a beneficial effect of the **BiTD**-RT combination. RT alone induced a 1.8-fold decrease in size, while combining RT with **BiTD** liposomes further enhanced this effect, leading to a 2.2-fold reduction (Figure 7B–C), with a significantly reduced spheroid growth curve. Assessment of viability revealed that RT alone never reduced viability below 80%, whereas the addition of **BiTD** liposomes produced a clear concentration-dependent decrease, reaching values as low as 60% at the highest **BiTD** concentrations (Figure 7D).

Given these heterogeneous responses between the two models, a third model was included, in which spheroids were established from p53 wild-type SW1990 cells. This model did not tolerate the extensive washing as in the PANC-1 and MIA PaCa-2 models, so a luminescence-based viability assay was used. Spheroids were incubated with 2.5 mol % **BiTD** liposomes at varying lipid concentrations. At 24 h post-radiotherapy (8 Gy), none of these concentrations demonstrated any notable treatment effects. However, clear reductions in spheroid viability were observed at 96h postradiotherapy. Interestingly, the result followed an inverse dose–response trend, where the lowest 0.1 mM lipid concentration yielded the strongest reduction in viability (Figure 7E,F). These results suggest that **BiTD**-loaded liposomes are capable of reducing SW1990 spheroid growth, which is best observed following several days of incubation post-treatment.

Together, these results demonstrate that **BiTD**-loaded liposomes are nontoxic in the absence of irradiation, while enhancing radiotherapeutic responses against radiotherapy-resistant pancreatic cancer spheroids. Thus, while model-dependent, these findings confirm the potential of **BiTD** liposomes as enhancers of radiotherapy.

In this study, we investigated the radiosensitizing efficacy of a novel triple-decker system comprising three tetra(*t*-butyl)-phthalocyanines coordinated with two Bi atoms, using radiochemical and *in vitro* assays on 3D culture models. Multiple decker phthalocyanines with Bi have already been reported, primarily to evaluate their synthetic feasibility and structural properties; however, no direct applications have been described to date. In earlier studies, the synthetic methods primarily relied on high-temperature solid-state synthesis ($200 < T < 310$ °C), which efficiently yielded the compounds; however, the main critique in prior studies was the poor stability of the molecule and the difficulties concerning the isolation and purification of the desired compound.[42−44] In this study, we present a synthetic strategy of a triple-decker phthalocyanine system under milder conditions. This method not only simplified the reaction process but also included an effective purification strategy based on the molecular weights of the different products. While the exact structure of the compound could not be fully elucidated due to pronounced structural disorder arising from the variable positions of the *tert*-butyl groups, our analyses confirm the formation of a triple-decker system comprising three phthalocyanine units and two Bi atoms. The applied purification protocol was important to maintaining the stability of the molecule, while enabling efficient isolation. The process employs a reusable size exclusion chromatography column and incorporates solvent recovery through distillation, minimizing waste and enhancing the overall sustainability of the method. This highlights size exclusion chromatography as a robust and reliable approach for purifying structurally intricate and sensitive multidecker phthalocyanine systems.

Working with **BiTD** has presented challenges due to its instability, which varied depending on the solvent used and exposure to light. Ethanol, readily induced demetalation, even when the compound was stored in the dark, suggesting that solvent polarity and pH may significantly influence molecular stability. Notably, EtOH is a polar, protic solvent with a high dielectric constant (24.6) and strong hydrogen-bonding ability.[45] Its −OH group can act as both a hydrogen bond donor and acceptor, allowing direct interactions with metal centers and bridging atoms in macrocyclic complexes. Such interactions may destabilize the delicate metal–ligand assemblies of sandwich complexes like **BiTD**, facilitating

https://doi.org/10.1021/acsami.5c26335
ACS Appl. Mater. Interfaces 2026, 18, 16205−16221

aggregation, ligand exchange, or even partial hydrolysis and degradation. This is a feature already seen in sandwich-type phthalocyanines, usually caused by acid-induced demetalation, solvent coordination effects, aggregation-induced instability, and possible hydrolytic or oxidative decomposition if the solvent contains impurities.[31,46] Bulky substitutions and surfactants can mitigate some of these effects,[31,46] which might explain the influence of phospholipids on the stabilization of **BiTD**, making liposomes a suitable nano-delivery system for such complexes.

Upon X-ray irradiation, **BiTD** consistently promoted ROS generation, producing an ∼1.4-fold increase compared to empty liposomes, demonstrating its potential as a radiosensitizer. Notably, Bi nanoparticles are generally efficient in achieving radiation dose enhancement (∼3-fold higher Auger or photoelectron production) compared to other metals (i.e., Pt and Au), with a concentration up to 350 mg/g.[47] Concerning the mechanism by which BiTD improves ROS generation and radiotherapy outcomes, we initially considered the physical radiation dose-enhancement mechanism. This effect stems from X-ray photoelectric interactions with tissue and is particularly effective in the presence of high-Z elements. This effect is theoretically feasible and routinely investigated by Monte Carlo simulations for high-Z element complexes. One critical factor is the concentration of the high-Z elements; for radiation dose-enhancement to occur, local concentrations in excess of 1 mg/mL are required.[48] However, in our case, the BiTD complex (2 Bi atoms/molecule) at 0.025 mM in 100 μL equates to just 1.04 μg Bi (∼0.001 mg/g spheroid), far below concentrations typically used for yielding measurable DEF (>7 mg/g) using radiation sources in the range between 50 kVp and 330 kVp.[49,50] We thus conclude that the radiation dose-enhancement effect of our complexes was negligible, and support the notion that our observed outcomes align with chemical/biological radiosensitizing mechanisms.[11] Therefore, the underlying mechanism for **BiTD** is unlikely to be due to a radiation dose enhancement, particularly given the reactivity observed even at low concentrations (2.5 μM **BiTD**). Notably, porphyrinoids have been reported to act as RDT agents due to their peculiar molecular structure. Their electronic flexibility enables them to accept and donate electrons, which is tightly linked to their redox activity. This results in the direct interaction of these macrocyclic compounds with secondary particles (e.g., electron, photons) produced during radiotherapy, but also redox-active species, proteins or other macromolecules present within the cellular environment.[11] Cyclic voltammetry revealed that **BiTD** undergoes a greater number of oxidation and reduction processes compared to **tbPc**, in a range which render it more prone to behave as an SOD mimic and consequently potentially enter redox cycling with cellular metabolites such as ascorbate or NADPH, disrupting redox homeostasis. Moreover, radiotherapy itself may influence these redox processes: X-ray irradiation might generate electrons with sufficient energy to ionize the macrocycle. Consequently, **BiTD** could act as an electron donor or acceptor, thereby amplifying ROS production and contributing to local ionization events. DHE assays showed that in the presence of ascorbate, **BiTD** significantly enhanced radiation induced probe oxidation compared with DHE and ascorbic acid alone. Ascorbate is expected to readily scavenge radiotherapy-generated ROS, thereby limiting oxidative processes. However, the small but significant enhancement observed upon the addition of **BiTD** suggests a distinct mechanism beyond simple ROS scavenging. This effect is likely attributable to the ability of **BiTD** to participate in redox cycling, during which it can react with molecular oxygen and catalyze $O_2^{\bullet-}$ dismutation. Additional mechanistic assays, such as spectroelectrochemistry, time-resolved absorbance, or direct product analysis, could further elucidate the underlying redox chemistry. Nevertheless, the combination of fluorescence probe readouts and the independently measured redox potentials of **BiTD** strongly supports a redox-cycling mechanism in which this complex mediates ascorbate oxidation and thereby promotes DHE and APF oxidation under the applied conditions.

To place these findings in context, it is important to highlight that phthalocyanines have not yet been systematically investigated for redox-cycling reactivity toward O_2; however, related macrocycles such as Gd-texaphyrins[34,35] and numerous Mn-porphyrins are well documented to function as SOD-mimics and catalyze $O_2^{\bullet-}$ dismutation, thereby perturbing cellular redox homeostasis and achieving radiosensitization.[51] A rigorous quantitative comparison between these systems and the present phthalocyanines is complicated by differences in the solvent and reference electrodes. Nevertheless, Mn-porphyrin SOD mimics typically exhibit formal Mn(III/II) potentials of about +300 mV vs a normal hydrogen electrode (NHE) which lies between the potentials for $O_2^{\bullet-}$ oxidation (approximately −180 mV vs NHE) and reduction (approximately +890 mV vs NHE).[51] Under such conditions, the Mn center can both oxidize and reduce superoxide, enabling catalytic dismutation. In the present work, the redox potentials were referenced to $Ag/AgNO_3$ (0.01 M) in a nonaqueous medium; converting these values to the NHE scale indicates that most phthalocyanine redox events occur at substantially more negative or more positive potentials than those of the Mn-porphyrin SOD mimics. Using an estimated offset of about +0.55 V between $Ag/AgNO_3$ (0.01 M) and NHE in these solvents,[52] the **BiTD** oxidation at +0.01 V vs $Ag/AgNO_3$ corresponds to roughly +0.56 V vs NHE. This potential lies within the electrochemical window in which $O_2^{\bullet-}$ can be both generated and oxidized. Although the main cellular compartments are aqueous and these oxidative potentials were recorded in an organic solvent, making identical reactivity in bulk water unlikely, it should be noted that **BiTD** is embedded within a lipophilic membrane. Cells themselves contain multiple lipophilic compartments, which make comparable redox behavior more plausible in such environments.

Direct investigation of the redox potentials within liposomes is experimentally challenging. Nevertheless, the differences observed between **BiTD** and **tbPc** in both redox potentials and **DHE** oxidation provide evidence that **BiTD** could participate in oxygen redox cycling and potentially mimic certain aspects of SOD-like behavior. In contrast, **tbPc** (Table 1), which does not exhibit redox processes within this potential range, is considerably less likely to engage in such activity under comparable conditions.

In solution, **BiTD** demonstrated the potential to increase the ROS levels in combination with radiotherapy. *In vitro* assays demonstrated model-dependent variability in terms of radiotherapy enhancement. PANC-1 spheroids appeared to be more susceptible to radiotherapy, particularly in terms of spheroid size. Nonetheless, **BiTD** did not induce any significant enhancement compared to radiotherapy alone. In contrast, MIA PaCa-2 spheroids were stunted in growth and had a

https://doi.org/10.1021/acsami.5c26335
ACS Appl. Mater. Interfaces 2026, 18, 16205−16221

significantly reduced viability when radiotherapy was combined with **BiTD**.

The differences observed between PANC-1 and MIA PaCa-2 spheroids are likely related to different factors such as spheroid compactness and hypoxic conditions.[53] While in this study we do not evaluate the differences in oxygenation between the two spheroids, it has been reported that MIA PaCa-2 and Panc-1 spheroids display differential activation of hypoxia-associated pathways with distinct HIF-1α/TrpRS regulation. Notably, TrpRS isoform patterns suggest that MIA PaCa-2 cells exhibit a constitutive hypoxia-adapted phenotype, whereas Panc-1 cells retain inducible hypoxia responsiveness, consistent with their ∼17-fold lower TrpRS mRNA expression compared with MIA PaCa-2.[54] As reported in literature, such as in this study, spheroids architecture also showed distinct differences, Panc-1 formed compact aggregates, whereas MIA PaCa-2 form the large floating cell conglomerates, with a looser architecture that results in a slower onset and a less pronounced hypoxic core at comparable diameters.[54,55] Moreover, the differences in NBD-PC fluorescence observed between the two cell lines are likely related to this phenomenon. NBD-PC is commonly used as a fluorescent lipid probe to monitor membrane dynamics, lipid scrambling, and redox activity.[56,57] A decrease in its fluorescence typically indicates enhanced oxidative processes at the cellular level. In this study, MIA PaCa-2 showed a fluorescence intensity 1.7-fold lower compared with Panc-1 spheroids, therefore supporting the presence of enhanced oxidative stress or redox activity compared with Panc-1. Given that oxygen plays a central role in ROS generation as well as in maintaining cellular redox homeostasis, we hypothesize that the structural differences between these two spheroid models might likely account for the reduced efficacy of **BiTD** observed in PANC-1 spheroids. Additionally, **BiTD** has demonstrated redox potentials within the range of interaction with molecular oxygen. Such effects were previously shown to highly vary in terms of radiosensitization between cell lines.[58] Future investigations could further elucidate these redox processes *in vitro* and explore additional mechanisms of cell death, such as apoptosis.

Taken together, a phthalocyanine construct composed of three **tbPc** coordinated by two Bi atoms exhibited promising radiosensitizing properties, which was attributed to its enriched redox properties, compared to the metal- free **tbPc**. Notably, **BiTD**-loaded liposomes induced a modest but reproducible increase in ROS production (∼1.3-fold compared to empty liposomes), accompanied by a pronounced reduction in the spheroid area (∼2.2-fold) in MIA PaCa-2 spheroids. Such efficacies correspond well with reported radiotherapy fold-enhancements for various porphyrins (1.2−2.5 fold increases[11]), Au nanoparticles (1.1−3 fold increases[59]), Hf nanoparticles (1.2−1.8 fold increases[60]), and Bi nanoparticles (1.3−1.8 fold increases[61]). This overgeneralization of such results does not take into account particle concentrations, radiation regimes, models, or radiosensitizing mechanisms. Nonetheless, our findings align with these more established radiation therapy enhancing agents, with ample opportunity to improve the design and dosing of the current reported treatment approach. Future investigations on **BiTD** or related compounds should aim to further expand the redox window and explore, in greater depth, their photochemical and electrochemical behavior in the presence of cellular metabolites under irradiation. Such studies could also help identify other suitable metal centers for improved performance and specifically stability.

CONCLUSIONS

Improving radiotherapy with porphyrinoids is a promising approach, as radiosensitization may be achieved at concentrations beneath those of high-Z element nanoparticles used for radiation-dose enhancement. However, unlike porphyrins and texaphyrins, phthalocyanines remain largely unexplored for radiodynamic therapy. Here we report on a sandwich-type phthalocyanine coordinated with Bi and its ability to act as a radiosensitizer. Liposomal encapsulation provided an unexpected benefit in stabilizing such a complex while rendering it biocompatible, with negligible leaching in serum. These results highlight the potential of sandwich-type phthalocyanines as effective radiosensitizers. In contrast to classical monophthalocyanines, which showed no significant radiosensitizing effect, the sandwich-type architecture appears particularly promising. This behavior is likely attributable to their broader redox window, which enhances their capacity to accept and donate electrons during radiotherapy, thereby improving the therapeutic outcomes. Looking forward, a rigorous *in vivo* evaluation will be required to assess the translational potential of **BiTD**-loaded liposomes. First, since the therapeutic properties of these triple-decker complexes have not been studied before, it is imperative to study their tolerability in dose-dependent toxicity assessments following repeated administration. Quantitative blood chemistry assessment would inform on hemotoxicity and vital organ toxicity (e.g., liver, kidney). Specific histological assessment of organs would be informed by blood chemistry analyses. Second, pharmacokinetic profiling and biodistribution analyses in tumor-bearing mice are required to determine circulation time, tumor accumulation, and clearance pathways of the **BiTD**-loaded liposomes. While **BiTD** has little fluorescence, elemental analysis of Bi such as inductively coupled plasma mass spectrometry would be indispensable for such investigations. In the case that the biodistribution studies following intravenous injection reveal insufficient tumor accumulation of the **BiTD** complexes, intratumor injections could be considered. Although this procedure is more complex than intravenous injection, the approach is emerging in clinical studies for radiotherapy-enhancing agents for which high local concentrations are needed (e.g., NCT04892173, NCT05838729). While technically feasible for subcutaneous tumors in small animals, the treatment of orthotopic tumors would require an ultrasound guided system to place a diffusing delivery system with the target tissue. The final challenge is the design of the *in vivo* radiotherapy approach. For pancreatic cancers, radiotherapy is typically given as stereotactic radiation therapy, during which doses of 5−10 Gy are given every 1−2 days to reach a cumulative dose of approximately 50 Gy.[62] The angles of the radiation beams are altered at each fraction so that healthy tissue is spared in the process.[63] Studies on small animals have revealed that such doses are far too high for mouse models of pancreatic cancer, whereas 10 consecutive days of anesthesia and radiotherapy may pose ethical restrictions on such experimental designs. A more pragmatic approach involves delivering radiotherapy either as a single dose using an arc beam or as a limited number of fractions to achieve a comparable cumulative dose or biologically equivalent dose, with the latter accounting for interfraction tissue repair mechanisms. Previous experiments on mouse

https://doi.org/10.1021/acsami.5c26335
ACS Appl. Mater. Interfaces 2026, 18, 16205−16221

models of pancreatic cancer have yielded promising results in this aspect, suggesting that 25 Gy delivered via a single-arc is a proper dose for *in vivo* evaluation at 220 keV.[64] However, limited information exists about how the radiotherapy schedule impacts the efficacy of radiotherapy-enhancing agents. When properly conducted, these investigations will be highly valuable to validate **BiTD** as a potential RDT-agent. In conclusion, the present work provides a valuable formulation strategy and proof of concept for the application of metal phthalocyanine complexes as next-generation radiodynamic therapy agents.

■ ASSOCIATED CONTENT

Supporting Information

The Supporting Information is available free of charge at https://pubs.acs.org/doi/10.1021/acsami.5c26335.

Experimental details on the synthesis and characterization of **tbPc** and **BiTD**; liposome formulation conditions and stability studies; SAXS, UV−Vis, NMR, and Cryo-EM analyses; radiotherapy enhancement assays in pancreatic cancer spheroids; and Figures S1−S11 and Table 1 illustrating spectroscopic, structural, and biological characterization data (PDF)

■ AUTHOR INFORMATION

Corresponding Authors

Sofia Leo − *PorphyChem SAS, 21600 Longvic, France; Université de Grenoble-Alpes, Institute for Advanced Biosciences, INSERM U1209, CNRS UMR 5309, 38700 Grenoble, France;* Present Address: Secció de Química Orgànica, Facultat de Química, Universitat de Barcelona, Carrer Martí i Franquès 1−11, 08028 Barcelona, Spain; orcid.org/0009-0003-5929-7777; Email: sleo@ub.edu

Benoit Habermeyer − *PorphyChem SAS, 21600 Longvic, France*; Email: b.habermeyer@porphychem.com

Mans Broekgaarden − *Université de Grenoble-Alpes, Institute for Advanced Biosciences, INSERM U1209, CNRS UMR 5309, 38700 Grenoble, France;* orcid.org/0000-0002-9516-5048; Email: Mans.Broekgaarden@univ-grenoble-alpes.fr

Authors

Elena Murillo Vilella − *Université de Grenoble-Alpes, Institute for Advanced Biosciences, INSERM U1209, CNRS UMR 5309, 38700 Grenoble, France;* Present Address: Institut de Ciència de Materials de Barcelona (ICMAB-CSIC), Campus de la, Carrer dels Til·lers, s/n, 08193 Barcelona, Spain

Laura Contini − *Dipartimento di Chimica "Giacomo Ciamician", University of Bologna, 40129 Bologna, Italy*

Fabrizia Grepioni − *Dipartimento di Chimica "Giacomo Ciamician", University of Bologna, 40129 Bologna, Italy;* orcid.org/0000-0003-3895-0979

Romain Haudecoeur − *Department of Molecular Pharmacochemistry, Université de Grenoble-Alpes, 38041 Grenoble, France;* orcid.org/0000-0002-6271-4717

Pierre-Henri Lanoë − *Department of Molecular Chemistry, Université de Grenoble-Alpes, 38000 Grenoble, France;* orcid.org/0000-0003-2596-2305

Malika Kadri − *Université de Grenoble-Alpes, Institute for Advanced Biosciences, INSERM U1209, CNRS UMR 5309, 38700 Grenoble, France*

Marc-André Hograindleur − *European Synchrotron Radiation Facility, 38000 Grenoble, France*

Eaazhisai Kandiah − *European Synchrotron Radiation Facility, 38000 Grenoble, France*

Jean-Luc Coll − *Université de Grenoble-Alpes, Institute for Advanced Biosciences, INSERM U1209, CNRS UMR 5309, 38700 Grenoble, France;* orcid.org/0000-0002-2453-3552

Lucie Sancey − *Université de Grenoble-Alpes, Institute for Advanced Biosciences, INSERM U1209, CNRS UMR 5309, 38700 Grenoble, France;* orcid.org/0000-0002-0084-3775

Complete contact information is available at: https://pubs.acs.org/10.1021/acsami.5c26335

Author Contributions

S.L.: Carried out laboratory research including synthesis, characterization, liposome investigations, SAXS analysis, and *in vitro* testing; wrote the original draft and the final version of the manuscript. E.M.V.: Carried out laboratory research including liposome investigations and *in vitro* testing; contributed to writing the original draft. L.C.: Carried out laboratory research for crystallization studies. F.G.: Contributed to validation and investigation. R.H.: Contributed to writing (review and editing), validation, and supervision. P.-H.L.: Carried out laboratory research for cyclic voltammetry analysis. M.K.: Carried out laboratory research for *in vitro* testing. M.-A.H.: Carried out laboratory research for Cryo-EM analysis. E.K.: Carried out laboratory research for Cryo-EM analysis, contribute to writing (review and editing) J.-L.C.: Contributed to writing (review and editing), validation and investigation. L.S.: Contributed to writing (review and editing), validation, and supervision. B.H.: Contributed to writing (review and editing), validation, supervision, and funding acquisition. M.B.: Carried out laboratory research including liposome investigations and *in vitro* testing; contributed to writing (original draft and review and editing), validation, supervision, project administration, investigation, and funding acquisition.

Funding

Association Nationale de la Recherche et de la Technologie (CIFRE, 2021/1790), European Research Council Starting Grant (101078392)

Notes

The authors declare the following competing financial interest(s): Benoit Habermeyer is the CEO of PorphyChem SAS.

■ ACKNOWLEDGMENTS

This research was funded by the National Research and Technology Agency (ANRT, Association Nationale de la Recherche et de la Technologie), via an Industrial Convention for Training through Research (CIFRE, 2021/1790). In addition, this research was supported by the European Union M.B: (ERC STG, RADIOCONTROL, 101078392). Views and opinions expressed are, however, those of the authors only and do not necessarily reflect those of the European Union or the European Research Council Executive Agency. Neither the European Union nor the granting authority can be held responsible for them. The authors further express their gratitude to Aurelien Thureau (Synchrotron Soleil, Saint Auban, France), Pau Bernado (Centre de

Biologie Structurale, CNRS UMR 5048, INSERM U 1054, University of Montpellier, France), and Daniel Hermida Merino (European Synchrotron Radiation Facility, Grenoble, France) for their aid with the SAXS measurements and data interpretation.

■ ABBREVIATIONS

APF– aminophenyl fluorescein; **ATCC**– american type culture collection; **BiTD**– bismuth triple-decker phthalocyanine; **CF**– 5(6)-carboxyfluorescein; **Chol**– cholesterol; **CV**– cyclic voltammetry; **DHE**– dihydroethidium; **DLS**– dynamic light scattering; **DMEM**– Dulbecco's modified eagle medium; **DOPE**– 1,2-dioleoyl-*sn*-glycero-3-phosphoethanolamine; **DSPE-PEG**– *N*-(carbonyl-methoxypolyethylene glycol-2000)-1,2-distearoyl-*sn*-glycero-3-phosphoethanolamine; **DSPC**– 1,2-distearoyl-*sn*-glycero-3-phosphocholine; **EtOH**– ethanol; **FADH**– reduced flavin adenine dinucleotide; **FBS**– fetal bovine serum; **HEPES**– 2-[4-(2-hydroxyethyl)piperazin-1-yl]-ethanesulfonic acid; **MALDI-TOF**– matrix-assisted laser desorption/ionization time-of-flight; **MIA PaCa-2**– human pancreatic cancer cell line; **NADPH**– nicotinamide adenine dinucleotide phosphate (reduced form); **NBD-PC**– 1-palmitoyl-2-(6-[(7-nitro-2−1,3-benzoxadiazol-4-yl)amino]hexanoyl)-*sn*-glycero-3-phosphocholine; **NHE**– normal hydrogen electrode; **NMR**– nuclear magnetic resonance; **O_2**– superoxide **PBS**−Phosphate-buffered saline; **PDI**– polydispersity index; **PC**– phthalocyanine; **PANC-1**– human pancreatic cancer cell line; ***q***– scattering vector; **RDT**– radiodynamic therapy; **R_g**– radius of gyration; **ROS**– reactive oxygen species; **RT**– radiotherapy; **SARRP**– small Animal Radiation Research Platform; **SAXS**– small-angle X-ray scattering; **SEM**– standard error of the mean; **SOD**– superoxide dismutase; **tbPc**– tetra(*tert*-butyl)phthalocyanine; **$TBAPF_6$**– tetrabutylammonium hexafluorophosphate; **TEM**– transmission electron microscopy

■ REFERENCES

(1) Malvezzi, M.; Santucci, C.; Boffetta, P.; Collatuzzo, G.; Levi, F.; Vecchia, C. L.; Negri, E. European Cancer Mortality Predictions for the Year 2023 with Focus on Lung Cancer. *Ann. Oncol.* **2023**, *34* (4), 410−419.

(2) Qin, C.; Yang, G.; Yang, J.; Ren, B.; Wang, H.; Chen, G.; Zhao, F.; You, L.; Wang, W.; Zhao, Y. Metabolism of Pancreatic Cancer: Paving the Way to Better Anticancer Strategies. *Mol. Cancer* **2020**, *19* (1), No. 50, DOI: 10.1186/s12943-020-01169-7.

(3) Stoop, T. F.; Theijse, R. T.; Seelen, L. W. F.; Koerkamp, B. G.; van Eijck, C. H. J.; Wolfgang, C. L.; van Tienhoven, G.; van Santvoort, H. C.; Molenaar, I. Q.; Wilmink, J. W.; Chiaro, M. D.; Katz, M. H. G.; Hackert, T.; Besselink, M. G. Preoperative Chemotherapy, Radiotherapy and Surgical Decision-Making in Patients with Borderline Resectable and Locally Advanced Pancreatic Cancer. *Nat. Rev. Gastroenterol. Hepatol.* **2024**, *21* (2), 101−124.

(4) Janssen, Q. P.; van Dam, J. L.; Kivits, I. G.; Besselink, M. G.; van Eijck, C. H. J.; Homs, M. Y. V.; Nuyttens, J. J. M. E.; Qi, H.; van Santvoort, H. J.; Wei, A. C.; de Wilde, R. F.; Wilmink, J. W.; van Tienhoven, G.; Koerkamp, B. G. Added Value of Radiotherapy Following Neoadjuvant FOLFIRINOX for Resectable and Borderline Resectable Pancreatic Cancer: A Systematic Review and Meta-Analysis. *Ann. Surg. Oncol.* **2021**, *28* (13), 8297−8308.

(5) Versteijne, E.; Suker, M.; Groothuis, K.; Akkermans-Vogelaar, J. M.; Besselink, M. G.; Bonsing, B. A.; Buijsen, J.; Busch, O. R.; Creemers, G.-J. M.; van Dam, R. M.; Eskens, F. A. L. M.; Festen, S.; de Groot, J. W. B.; Groot Koerkamp, B.; de Hingh, I. H.; Homs, M. Y. V.; van Hooft, J. E.; Kerver, E. D.; Luelmo, S. A. C.; Neelis, K. J.; Nuyttens, J.; Paardekooper, G. M. R. M.; Patijn, G. A.; van der Sangen, M. J. C.; de Vos-Geelen, J.; Wilmink, J. W.; Zwinderman, A. H.; Punt, C. J.; van Eijck, C. H.; van Tienhoven, G. Preoperative Chemoradiotherapy Versus Immediate Surgery for Resectable and Borderline Resectable Pancreatic Cancer: Results of the Dutch Randomized Phase III PREOPANC Trial. *J. Clin. Oncol.* **2020**, *38* (16), 1763−1773.

(6) Versteijne, E.; van Dam, J. L.; Suker, M.; Janssen, Q. P.; Groothuis, K.; Akkermans-Vogelaar, J. M.; Besselink, M. G.; Bonsing, B. A.; Buijsen, J.; Busch, O. R.; Creemers, G.-J. M.; van Dam, R. M.; Eskens, F. A. L. M.; Festen, S.; de Groot, J. W. B.; Koerkamp, B. G.; de Hingh, I. H.; Homs, M. Y. V.; van Hooft, J. E.; Kerver, E. D.; Luelmo, S. A. C.; Neelis, K. J.; Nuyttens, J.; Paardekooper, G. M. R. M.; Patijn, G. A.; van der Sangen, M. J. C.; de Vos-Geelen, J.; Wilmink, J. W.; Zwinderman, A. H.; Punt, C. J.; van Tienhoven, G.; van Eijck, C. H. J. Neoadjuvant Chemoradiotherapy Versus Upfront Surgery for Resectable and Borderline Resectable Pancreatic Cancer: Long-Term Results of the Dutch Randomized PREOPANC Trial. *J. Clin. Oncol.* **2022**, *40* (11), 1220−1230.

(7) Song, G.; Cheng, L.; Chao, Y.; Yang, K.; Liu, Z. Emerging Nanotechnology and Advanced Materials for Cancer Radiation Therapy. *Adv. Mater.* **2017**, *29* (32), No. 1700996, DOI: 10.1002/adma.201700996.

(8) Fulbert, C. A.; Chaput, F.; Stelse-Masson, S.; Henry, M.; Chovelon, B.; Bohic, S.; Brueckner, D.; Garrevoet, J.; Moriscot, C.; Gallet, B.; Vollaire, J.; Nicoud, O.; Lerouge, F.; Denis-Quanquin, S.; Jaurand, X.; Jacquet, T.; Nomezine, A.; Josserand, V.; Coll, J.; Ravanat, J.; Elleaume, H.; Bulin, A. Nanoscintillator Coating: A Key Parameter That Strongly Impacts Internalization, Biocompatibility, and Therapeutic Efficacy in Pancreatic Cancer Models. *Small Sci.* **2024**, *4* (5), No. 2400041, DOI: 10.1002/smsc.202400041.

(9) Stelse-Masson, S.; Lytvynenko, X.; Bedregal-Portugal, K.; Aubrun, C.; Lavaud, M.; Kadri, M.; Jacquet, T.; Moriscot, C.; Gallet, B.; Chovelon, B.; Coll, J.-L.; Ravanat, J.-L.; Mihóková, E.; Cuba, V.; Elleaume, H.; Bulin, A.-L. Combined Physical and Biological Contributions to Radiotherapy Enhancement by Lu-Based Nanoscintillators in Pancreatic Cancer Models. *Nanotheranostics* **2025**, *9* (3), 199−215.

(10) Varzandeh, M.; Sabouri, L.; Mansouri, V.; Gharibshahian, M.; Beheshtizadeh, N.; Hamblin, M. R.; Rezaei, N. Application of Nano-Radiosensitizers in Combination Cancer Therapy. *Bioeng. Transl. Med.* **2023**, *8* (3), No. e10498, DOI: 10.1002/btm2.10498.

(11) Leo, S.; Gutierrez, N. M. C.; Bulin, A. L.; Coll, J. L.; Sancey, L.; Habermeyer, B.; Broekgaarden, M. The Physicochemical and Biochemical Mechanisms of Porphyrinoid-Mediated Radiodynamic Therapy. *Eur. J. Med. Chem.* **2025**, *296*, No. 117861.

(12) Ali, H.; van Lier, J. E. Metal Complexes as Photo- and Radiosensitizers. *Chem. Rev.* **1999**, *99* (9), 2379−2450.

(13) Kadish, K. M.; Smith, K. M.; Guilard, R. The Porphyrin Handbook. In *Phthalocyanines: Properties and Materials*; Academic Press, 2012; Vol. *17* DOI: 10.1016/C2009-0-22720-6.

(14) Jiang, J.; Liu, W.; Arnold, D. P. Sandwich Complexes of Naphthalocyanine with the Rare Earth Metals. *J. Porphyrins Phthalocyanines* **2003**, *07*, 459−473, DOI: 10.1142/S1088424603000598.

(15) Tang, X.; Liu, Q.; Wei, C.; Lv, X.; Jin, Z.; Chen, Y.; Jiang, J. Advances in Gas Sensors of Tetrapyrrolato-Rare Earth Sandwich-Type Complexes — Commemorating the 100th Anniversary of the Birth of Academician Guangxian Xu. *J. Rare Earths* **2021**, *39*, 113−120.

(16) Tomoda, H.; Saito, S.; Shiraishi, S. synthesis of metallophthalocyanines from phthalonitrile with strong organic bases. *Chem. Lett.* **1983**, *12* (3), 313−316.
(17) *The Porphyrin Handbook—Phthalocyanines: Synthesis*; Kadish, K. M.; Smith, K. M.; Guilard, R., Eds.; Academic Press, 2003; Vol. *15* DOI: 10.1016/C2009-0-22718-8.
(18) Kandiah, E.; Giraud, T.; de Maria Antolinos, A.; Dobias, F.; Effantin, G.; Flot, D.; Hons, M.; Schoehn, G.; Susini, J.; Svensson, O.; Leonard, G. A.; Mueller-Dieckmann, C. CM01: A Facility for Cryo-Electron Microscopy at the European Synchrotron. *Acta Crystallogr., Sect. D:Struct. Biol.* **2019**, *75* (6), 528−535.
(19) Gutierrez, N. M. C.; Le Clainche, T.; Bulin, A. L.; Leo, S.; Kadri, M.; Abdelhamid, A. G. A.; Pujol-Solé, N.; Obaid, G.; Hograindleur, M. A.; Gardette, V.; Busser, B.; Motto-Ros, V.; Josserand, V.; Henry, M.; Sancey, L.; Hurbin, A.; Elleaume, H.; Kandiah, E.; Guével, X. L.; Coll, J. L.; Broekgaarden, M. Engineering Radiocatalytic Nanoliposomes with Hydrophobic Gold Nanoclusters for Radiotherapy Enhancement. *Adv. Mater.* **2024**, *36* (50), No. 2404605, DOI: 10.1002/adma.202404605.
(20) Setsukinai, K. i.; Urano, Y.; Kakinuma, K.; Majima, H. J.; Nagano, T. Development of Novel Fluorescence Probes That Can Reliably Detect Reactive Oxygen Species and Distinguish Specific Species. *J. Biol. Chem.* **2003**, *278* (5), 3170−3175, DOI: 10.1074/jbc.M209264200.
(21) Cohn, C. A.; Pedigo, C. E.; Hylton, S. N.; Simon, S. R.; Schoonen, M. A. Evaluating the Use of 3′-(p-Aminophenyl) Fluorescein for Determining the Formation of Highly Reactive Oxygen Species in Particle Suspensions. *Geochem. Trans.* **2009**, *10* (1), No. 8.
(22) Chen, R. F.; Knutson, J. R. Mechanism of Fluorescence Concentration Quenching of Carboxyfluorescein in Liposomes: Energy Transfer to Nonfluorescent Dimers. *Anal. Biochem.* **1988**, *172* (1), 61−77.
(23) Bulin, A. L.; Broekgaarden, M.; Hasan, T. Comprehensive High-Throughput Image Analysis for Therapeutic Efficacy of Architecturally Complex Heterotypic Organoids. *Sci. Rep.* **2017**, *7* (1), No. 16645, DOI: 10.1038/s41598-017-16622-9.
(24) Deer, E. L.; González-Hernández, J.; Coursen, J. D.; Shea, J. E.; Ngatia, J.; Scaife, C. L.; Firpo, M. A.; Mulvihill, S. J. Phenotype and Genotype of Pancreatic Cancer Cell Lines. *Pancreas* **2010**, *39* (4), 425−435.
(25) Sugimoto, H.; Nakamura, M.; Yoda, H.; Hiraoka, K.; Shinohara, K.; Sang, M.; Fujiwara, K.; Shimozato, O.; Nagase, H.; Ozaki, T. Silencing of RUNX2 Enhances Gemcitabine Sensitivity of P53-Deficient Human Pancreatic Cancer AsPC-1 Cells through the Stimulation of TAp63-Mediated Cell Death. *Cell Death Discovery* **2015**, *1* (1), No. 15010.
(26) Janczak, J.; Kubiak, R.; Richter, J.; Fuess, H. Bismuth Triple-Decker Phthalocyanine: Synthesis and Structure. *Polyhedron* **1999**, *18* (21), 2775−2780.
(27) Polovkova, M. A.; Martynov, A. G.; Birin, K. P.; Nefedov, S. E.; Gorbunova, Y. G.; Tsivadze, A. Y. Determination of the Structural Parameters of Heteronuclear (Phthalocyaninato)Bis-(Crownphthalocyaninato)Lanthanide(III) Triple-Deckers in Solution by Simultaneous Analysis of NMR and Single-Crystal X-Ray Data. *Inorg. Chem.* **2016**, *55* (18), 9258−9269.
(28) Ishikawa, N. Electronic Structures and Spectral Properties of Double- and Triple-Decker Phthalocyanine Complexes in a Localized Molecular Orbital View. *J. Porphyr. Phthalocyanines* **2001**, *5* (1), 87−101.
(29) Iida, N.; Tanaka, K.; Tokunaga, E.; Takahashi, H.; Shibata, N. Regioisomer-Free C_{4h} B-Tetrakis(Tert -butyl)Metallo-phthalocyanines: Regioselective Synthesis and Spectral Investigations. *ChemistryOpen* **2015**, *4* (2), 102−106.
(30) Cook, M. J.; Chambrier, I.; White, G. F.; Fourie, E.; Swarts, J. C. Electrochemical and EPR Studies of Two Substituted Bis-Cadmium Tris-Phthalocyanine Complexes: Elucidation of Unexpectedly Different Free-Radical Character. *Dalton Trans.* **2009**, No. 7, 1136−1144.
(31) Cerný, J.; Dokládalová, L.; Horáková, P.; Lyčka, A.; Mikysek, T.; Bureš, F. Preparation and Characterization of Novel Double-Decker Rare-Earth Phthalocyanines Substituted with 5-Bromo-2-Thienyl Groups. *Chem. Cent. J.* **2017**, *11* (1), No. 31, DOI: 10.1186/s13065-017-0260-x.
(32) Horii, Y.; Damjanović, M.; Ajayakumar, M. R.; Katoh, K.; Kitagawa, Y.; Chibotaru, L.; Ungur, L.; Mas-Torrent, M.; Wernsdorfer, W.; Breedlove, B. K.; Enders, M.; Veciana, J.; Yamashita, M. Highly Oxidized States of Phthalocyaninato Terbium(III) Multiple-Decker Complexes Showing Structural Deformations, Biradical Properties and Decreases in Magnetic Anisotropy. *Chem. − Eur. J.* **2020**, *26* (39), 8621−8630.
(33) Akbarzadeh, A.; Rezaei-Sadabady, R.; Davaran, S.; Joo, S. W.; Zarghami, N.; Hanifehpour, Y.; Samiei, M.; Kouhi, M.; Nejati-Koshki, K. Liposome: Classification, Preparation, and Applications. *Nanoscale Res. Lett.* **2013**, *8* (1), No. 102, DOI: 10.1186/1556-276X-8-102.
(34) Hashemzadeh, H.; Javadi, H.; Darvishi, M. H. Study of Structural Stability and Formation Mechanisms in DSPC and DPSM Liposomes: A Coarse-Grained Molecular Dynamics Simulation. *Sci. Rep.* **2020**, *10* (1), No. 1837, DOI: 10.1038/s41598-020-58730-z.
(35) Caselli, L.; Conti, L.; de Santis, I.; Berti, D. Small-Angle X-Ray and Neutron Scattering Applied to Lipid-Based Nanoparticles: Recent Advancements across Different Length Scales. *Adv. Colloid Interface Sci.* **2024**, *327*, No. 103156.
(36) Khan, M. M. T.; Martell, A. E. Metal Ion and Metal Chelate Catalyzed Oxidation of Ascorbic Acid by Molecular Oxygen. II. Cupric and Ferric Chelate Catalyzed Oxidation. *J. Am. Chem. Soc.* **1967**, *89* (26), 7104−7111.
(37) Shen, J.; Griffiths, P. T.; Campbell, S. J.; Utinger, B.; Kalberer, M.; Paulson, S. E. Ascorbate Oxidation by Iron, Copper and Reactive Oxygen Species: Review, Model Development, and Derivation of Key Rate Constants. *Sci. Rep.* **2021**, *11* (1), No. 7417.
(38) Krishnamurthy, H. K.; Pereira, M.; Rajavelu, I.; Jayaraman, V.; Krishna, K.; Wang, T.; Bei, K.; Rajasekaran, J. J. Oxidative Stress: Fundamentals and Advances in Quantification Techniques. *Front. Chem.* **2024**, *12*, No. 1470458, DOI: 10.3389/fchem.2024.1470458.
(39) Gradiz, R.; Silva, H. C.; Carvalho, L.; Botelho, M. F.; Mota-Pinto, A. MIA PaCa-2 and PANC-1 − Pancreas Ductal Adenocarcinoma Cell Lines with Neuroendocrine Differentiation and Somatostatin Receptors. *Sci. Rep.* **2016**, *6* (1), No. 21648.
(40) Hammond, J.; Richards, C. J.; Ko, Y.; Jonker, T.; Åberg, C.; Roos, W. H.; Lira, R. B. Membrane Fusion-Based Drug Delivery Liposomes Transiently Modify the Material Properties of Synthetic and Biological Membranes. *Small* **2025**, *21* (12), No. 2408039, DOI: 10.1002/smll.202408039.
(41) Cavo, M.; Cave, D. D.; D'Amone, E.; Gigli, G.; Lonardo, E.; del Mercato, L. L. A Synergic Approach to Enhance Long-Term Culture and Manipulation of MiaPaCa-2 Pancreatic Cancer Spheroids. *Sci. Rep.* **2020**, *10* (1), No. 10192.
(42) Benihya, K.; Mossoyan-Déneux, M.; Hahn, F.; Boucharat, N.; Terzian, G. Synthesis, Crystal Structure and Spectral Characterization, of a New Phase of Tris(Phthalocyaninato)Dibismuth(III), Bi2(Pc)3. *Eur. J. Inorg. Chem.* **2000**, 1771−1779.
(43) Kubiak, R.; Ejsmont, K. Crystal Structure of a Novel Bismuth Phthalocyanine-Bismuth Iodide Complex. *J. Mol. Struct.* **1999**, *474*, 275−281.
(44) Janczak, J.; Kubiak, R.; Richter, J.; Fuess, H. Bismuth Triple-Decker Phthalocyanine: synthesis and Structure. *Polyhedron* **1999**, *18* (21), 2775−2780.
(45) Myers, B. J. Common Solvents Used in Organic Chemistry: Table of Properties. https://organicchemistrydata.org/solvents/ https://organicchemistrydata.org/solvents/ (accessed 2025−10−15).
(46) Pinnock, J.; Hansen, K.; Pelmuş, M.; Fadeev, A. Y. The Unexpected High Solubility of Fluorinated Zinc Phthalocyanines in Aqueous Solutions and Their Use for the Preparation of Photodynamic Coatings on Various Substrates. *Langmuir* **2025**, *41* (12), 8202−8213.

(47) Hossain, M.; Su, M. Nanoparticle Location and Material-Dependent Dose Enhancement in X-Ray Radiation Therapy. *J. Phys. Chem. C* **2012**, *116* (43), 23047−23052.
(48) Roeske, J. C.; Nuñez, L.; Hoggarth, M.; Labay, E.; Weichselbaum, R. R. Characterization of the Theorectical Radiation Dose Enhancement from Nanoparticles. *Technol. Cancer Res. Treat.* **2007**, *6* (5), 395−401.
(49) Hossain, M.; Su, M. Nanoparticle Location and Material-Dependent Dose Enhancement in X-Ray Radiation Therapy. *J. Phys. Chem. C* **2012**, *116* (43), 23047−23052.
(50) Gebremariam, T.; Geraily, G.; Longo, F.; Gholami, S. Radiation Dose Escalation by Injecting Bismuth, Gold and Platinum Nanoparticles into a Tumour during High Dose Rate 192Ir Brachytherapy: A Monte Carlo Study. *Radiat. Environ. Biophys.* **2025**, *64* (2), 303−310.
(51) Batinic-Haberle, I.; Tovmasyan, A.; Roberts, E. R. H.; Vujaskovic, Z.; Leong, K. W.; Spasojevic, I. SOD Therapeutics: Latest Insights into Their Structure-Activity Relationships and Impact on the Cellular Redox-Based Signaling Pathways. *Antioxid. Redox Signaling* **2014**, *20* (15), 2372−2415.
(52) Pavlishchuk, V. V.; Addison, A. W. Conversion Constants for Redox Potentials Measured versus Different Reference Electrodes in Acetonitrile Solutions at 25°C. *Inorg. Chim. Acta* **2000**, *298* (1), 97−102.
(53) Wishart, G.; Gupta, P.; Nisbet, A.; Schettino, G.; Velliou, E. On the Evaluation of a Novel Hypoxic 3d Pancreatic Cancer Model as a Tool for Radiotherapy Treatment Screening. *Cancers* **2021**, *13* (23), No. 6080.
(54) Paley, E. L.; Paley, D. E.; Merkulova-Rainon, T.; Subbarayan, P. R. Hypoxia Signature of Splice Forms of Tryptophanyl-TRNA Synthetase Marks Pancreatic Cancer Cells with Distinct Metastatic Abilities. *Pancreas* **2011**, *40* (7), 1043−1056.
(55) Doctor, A.; Laube, M.; Meister, S.; Kiss, O. C.; Kopka, K.; Hauser, S.; Pietzsch, J. Combined PET Radiotracer Approach Reveals Insights into Stromal Cell-Induced Metabolic Changes in Pancreatic Cancer In Vitro and In Vivo. *Cancers* **2024**, *16* (19), No. 3393.
(56) Alakoskela, J.-M. I.; Kinnunen, P. K. J. Control of a Redox Reaction on Lipid Bilayer Surfaces by Membrane Dipole Potential. *Biophys. J.* **2001**, *80* (1), 294−304.
(57) Niu, H.; Maruoka, M.; Noguchi, Y.; Kosako, H.; Suzuki, J. Phospholipid Scrambling Induced by an Ion Channel/Metabolite Transporter Complex. *Nat. Commun.* **2024**, *15* (1), No. 7566.
(58) Chatterjee, A.; Zhu, Y.; Tong, Q.; Kosmacek, E.; Lichter, E.; Oberley-Deegan, R. The Addition of Manganese Porphyrins during Radiation Inhibits Prostate Cancer Growth and Simultaneously Protects Normal Prostate Tissue from Radiation Damage. *Antioxidants* **2018**, *7* (1), No. 21.
(59) Rosa, S.; Connolly, C.; Schettino, G.; Butterworth, K. T.; Prise, K. M. Biological Mechanisms of Gold Nanoparticle Radiosensitization. *Cancer Nanotechnol.* **2017**, *8* (1), No. 2.
(60) Zhang, P.; Marill, J.; Darmon, A.; Anesary, N. M.; Lu, B.; Paris, S. NBTXR3 Radiotherapy-Activated Functionalized Hafnium Oxide Nanoparticles Show Efficient Antitumor Effects Across a Large Panel of Human Cancer Models. *Int. J. Nanomed.* **2021**, *16*, 2761−2773.
(61) Tarighatnia, A.; Amanzadeh, M.; Darvish, L.; Amraee, A.; Ghojazadeh, M.; Aghanejad, A. Radiosensitivity Enhancement of Bismuth-Based Nanoparticles in Radiotherapy: A Systematic Review and Meta-Analysis. *Comput. Biol. Chem.* **2025**, *120*, No. 108767.
(62) Stoop, T. F.; Theijse, R. T.; Seelen, L. W. F.; Koerkamp, B. G.; van Eijck, C. H. J.; Wolfgang, C. L.; van Tienhoven, G.; van Santvoort, H. C.; Molenaar, I. Q.; Wilmink, J. W.; Chiaro, M. D.; Katz, M. H. G.; Hackert, T.; Besselink, M. G. Preoperative Chemotherapy, Radiotherapy and Surgical Decision-Making in Patients with Borderline Resectable and Locally Advanced pancreatic Cancer. *Nat. Rev. Gastroenterol. Hepatol.* **2024**, *21* (2), 101−124.
(63) Baumann, M.; Krause, M.; Overgaard, J.; Debus, J.; Bentzen, S. M.; Daartz, J.; Richter, C.; Zips, D.; Bortfeld, T. Radiation Oncology in the Era of Precision Medicine. *Nat. Rev. Cancer* **2016**, *16* (4), 234−249.
(64) Dobiasch, S.; Kampfer, S.; Steiger, K.; Schilling, D.; Fischer, J.; Schmid, T.; Weichert, W.; Wilkens, J.; Combs, S. Histopathological Tumor and Normal Tissue Responses after 3D-Planned Arc Radiotherapy in an Orthotopic Xenograft Mouse Model of Human Pancreatic Cancer. *Cancers* **2021**, *13* (22), No. 5656.

https://doi.org/10.1021/acsami.5c26335
ACS Appl. Mater. Interfaces 2026, 18, 16205−16221